Omics-based label-free metabolic flux inference reveals dysregulation of glucose metabolism in liver associated with obesity

Authors

Saori Uematsu[1], Satoshi Ohno[2,3], Kaori Y. Tanaka[1], Atsushi Hatano[4], Toshiya Kokaji[3], Yuki Ito[1,5], Hiroyuki Kubota[5], Ken-ichi Hironaka[3], Yutaka Suzuki[1], Masaki Matsumoto[4], Keiichi I. Nakayama[6], Akiyoshi Hirayama[7], Tomoyoshi Soga[7], Shinya Kuroda[1,2,3,8*]

Affiliations

[1]Department of Computational Biology and Medical Sciences, Graduate School of Frontier Sciences, The University of Tokyo, 5-1-5 Kashiwanoha, Kashiwa, Chiba 277-8562, Japan.

[2]Molecular Genetic Research Laboratory, Graduate School of Science, The University of Tokyo, 7-3-1 Hongo, Bunkyo-ku, Tokyo, Japan

[3]Department of Biological Sciences, Graduate School of Medicine, The University of Tokyo, 7-3-1 Hongo, Bunkyo-ku, Tokyo 113-0033, Japan.

[4]Department of Omics and Systems Biology, Graduate School of Medicinal and Dental Sciences, Niigata University, 757 Ichibancho, Asahimachi-dori, Chuo-ku, Niigata City, Niigata 951-8510, Japan

[5]Division of Integrated Omics, Research Center for Transomics Medicine, Medical Institute of Bioregulation, Kyushu University, 3-1-1 Maidashi, Higashi-ku, Fukuoka 812-8582, Japan.

[6]Department of Molecular and Cellular Biology, Medical Institute of Bioregulation, Kyushu University, 3-1-1 Maidashi, Higashi-ku, Fukuoka 812-8582, Japan.

[7]Institute for Advanced Biosciences, Keio University, 246-2 Mizukami, Kakuganji, Tsuruoka, Yamagata 997-0052, Japan.

[8]Lead Contact

*Correspondence to: skuroda@bs.s.u-tokyo.ac.jp (S.K.)

SUMMARY

Glucose homeostasis is maintained by modulating metabolic flux through various metabolic pathways in metabolic organs such as liver, and a change in metabolic flux is regulated by enzymes and metabolites. Obesity represents dysregulation of the glucose homeostasis, but changes in metabolic fluxes and their regulations associated with obesity have not been fully understood. Here we introduce Omics-based Metabolic flux Estimation without Labeling for Extended Trans-omic analysis (OMELET), an approach that uses metabolomic, proteomic and transcriptomic data to identify changes in metabolic flux, and to quantify contributions of metabolites, enzymes and transcripts to the changes in metabolic flux. We identified obesity-associated increases in metabolic fluxes through gluconeogenesis and pyruvate cycle in fasting *ob*/*ob* mice. The increased metabolic flux through gluconeogenesis was contributed by increased transcripts, while that through pyruvate cycle by increased transcripts and substrates. OMELET provided quantitative insights into alteration and dysregulation of metabolic flux in liver associated with obesity.

Highlights

- We created OMELET to infer metabolic flux and its regulation from multi-omic data.
- Gluconeogenic and pyruvate cycle flux increased in fasting *ob*/*ob* mice.
- Increased gluconeogenic fluxes in *ob*/*ob* mice were caused by increased transcripts.
- Increased pyruvate cycle fluxes were led by increased transcripts and substrates.

Keywords

Trans-omics, multi-omics, metabolic flux, gluconeogenesis, pyruvate cycle, mathematical modeling, Bayesian modeling, liver, obesity

53 **INTRODUCTION**

54 Glucose homeostasis is tightly regulated to meet the energy requirements of vital organs
55 and maintain health. Dysregulation of glucose homeostasis leads to metabolic diseases
56 such as obesity and type 2 diabetes (Kahn et al., 2006). The liver plays a central role in
57 glucose homeostasis by regulating various pathways of glucose metabolism, including
58 gluconeogenesis and glycolysis (Han et al., 2016). The importance of the liver in the
59 pathophysiology of obesity has been widely recognized (Roden and Shulman, 2019).
60 Fasting hyperglycemia in obesity is attributed to altered glucose metabolism in liver due
61 to insulin resistance. Because of the complex nature of the pathophysiology of glucose
62 metabolism in liver associated with obesity, the dysregulation of the whole system cannot
63 be understood just by integrating the results of individual experiments from different
64 conditions. Therefore, it is necessary to investigate alterations and dysregulation of
65 glucose metabolism in liver associated with obesity using the data obtained under the
66 same conditions.

67 Metabolic flux, a rate of turnover of molecules through a metabolic pathway, is
68 a direct measure of the activity of the metabolic pathway rather than the amounts of
69 metabolites *per se* (Jang et al., 2018). The standard method for measuring metabolic flux
70 is an isotopic labeling experiment, in which isotopic tracers are introduced into cells or
71 living animals (Hasenour et al., 2015, 2020). One of the problems with the application of
72 isotope labeling experiments to living animals is that the addition of isotopic tracers can
73 perturb metabolic flux of interest, resulting in the different metabolic states (Previs and
74 Kelley, 2015). For example, when ^{13}C-propionate or ^{13}C-lactate is used as isotopic tracer
75 for measurement of gluconeogenic flux, the measured metabolic fluxes were different
76 because the administration of ^{13}C-propionate induced an artificial increase in the
77 metabolic flux through pyruvate cycle (Perry et al., 2016). Therefore, the addition of
78 isotopic tracers inevitably induces artificial changes in metabolic flux. To avoid the
79 effects of the addition of isotopic tracers, a method to infer metabolic flux without using

isotopic tracers is needed to be developed.

Metabolic flux is controlled by multiple regulators: enzymes, substrates, products and cofactors. Enzymes are regulated by allosteric effectors and other factors such as post-translational modifications of enzymes. The amounts of enzymes are determined by the amounts of transcripts encoding the corresponding enzymes and other factors such as translation and protein degradation. To investigate metabolic flux and its complex regulation, the amounts of regulators of metabolic flux should be simultaneously measured. The amounts of enzymes can be measured by proteomics, transcripts of enzymes by transcriptomics, and the amounts of substrates, products, cofactors and allosteric effectors by metabolomics. The simultaneously obtained multi-omic data can be used to analyze the regulation of metabolic flux. We have proposed a trans-omic analysis for the construction of a global biochemical network using the simultaneously obtained multi-omic data based on direct molecular interaction (Egami et al., 2021; Kawata et al., 2018; Kokaji et al., 2020; Yugi et al., 2014, 2016), but metabolic fluxes have not been inferred. To analyze the regulation of metabolic flux, we developed a kinetic trans-omic analysis using isotopic labeling experiments, and inferred metabolic flux together with contributions of regulators to changes in metabolic flux across multiple omic layers (Ohno et al., 2020). However, a method to analyze trans-omic regulation of metabolic flux using multi-omic data without using isotopic tracers has not been developed.

Here we present a method that we termed as Omics-based Metabolic flux Estimation without Labeling for Extended Trans-omic analysis (OMELET). OMELET infers metabolic fluxes in each condition from metabolomic, proteomic and transcriptomic data, which are simultaneously obtained from the same individual mice, identifies changes in metabolic flux between the conditions, and quantifies contributions of regulators to the changes in metabolic flux. We obtained metabolomic, proteomic and transcriptomic data from livers of wild-type (WT) and leptin-deficient obese (*ob*/*ob*) mice

at fasting state and four hours after oral glucose administration. By applying OMELET to the experimental data, we inferred metabolic fluxes in each condition. At fasting state, metabolic fluxes through reactions in gluconeogenesis and pyruvate cycle increased in *ob*/*ob* mice compared to WT mice. We quantified contributions of regulators to changes in metabolic flux between the conditions. The increased metabolic fluxes through reactions in gluconeogenesis were caused by increased transcripts. In contrast, the increased metabolic fluxes through pyruvate kinase (PK) and phosphoenolpyruvate carboxykinase (PEPCK) in pyruvate cycle were caused by increased transcripts and substrates, respectively. We also quantified the contributions of regulators to changes in metabolic flux by oral glucose administration. By oral glucose administration, metabolic flux through PK decreased in both WT and *ob*/*ob* mice, however, decreased PK flux was caused by increased ATP as an allosteric inhibitor in WT mice, whereas that was caused by its decreased transcript in *ob*/*ob* mice. Thus, OMELET provided quantitative insights into alteration and dysregulation of metabolic flux associated with obesity without using isotopic tracers.

RESULTS

Overview of OMELET

In this study, we developed a method that we termed as Omics-based Metabolic flux Estimation without Labeling for Extended Trans-omic analysis (OMELET) to infer metabolic flux using multi-omic data without using isotopic tracers, identify changes in metabolic flux between conditions, and quantify contributions of regulators to the changes in metabolic flux (Figure 1).

We orally administered glucose to 16 hours fasting WT and *ob*/*ob* mice, and collected livers at zero and four hours after oral glucose administration (Figure 1: Experimental data). We had four conditions: WT at fasting state, WT after oral glucose administration, *ob*/*ob* at fasting state and *ob*/*ob* after oral glucose administration. In each condition, we measured the amounts of metabolites, proteins and transcripts of liver samples from the same individual mice.

By applying OMELET to the experimental data, we inferred metabolic fluxes in the glucose metabolism in each condition, and identified changes in metabolic flux between the conditions (Figure 1: Step 1). A metabolic flux refers to the rate of turnover of a metabolite, and is a direct measure of the activity of the metabolic pathway. We focused on reactions in the glucose metabolism, and inferred metabolic fluxes through the reactions in glycogenolysis, gluconeogenesis, lactate and alanine metabolism, pyruvate cycle and TCA cycle (Figure 1; Table S1).

We considered regulators of metabolic flux including transcripts, unaccounted enzyme regulators, substrate, product, cofactor, allosteric effector and unaccounted flux regulators. The changes in metabolic fluxes between conditions are caused by the changes of regulators. To investigate which regulators caused changes in metabolic flux between the conditions, we quantified contributions of the regulators to changes in metabolic flux between the conditions (Figure 1: Step 2). Contributions of enzyme referred to those of the amounts of proteins, which were the sum of those of transcript and unaccounted

149 enzyme regulators, representing the contributions of gene expression of the enzyme and
150 unaccounted regulation for protein expression of the enzyme, respectively.
151 By integrating changes in the experimental data, changes in metabolic flux
152 (Figure 1: Step 1), and contributions of the regulators to the changes in metabolic flux
153 between the conditions (Figure 1: Step 2), we constructed a quantitative trans-omic
154 network for changes in metabolic flux in the glucose metabolism in liver (Figure 1: Step
155 3).
156
157 **Metabolomic, proteomic and transcriptomic data in the glucose metabolism in liver**
158 **of WT and *ob*/*ob* mice at fasting state and after oral glucose administration**
159 We obtained metabolomic, proteomic and transcriptomic data from livers of WT and
160 *ob*/*ob* mice at fasting state and four hours after oral glucose administration (Figure 2),
161 where the blood glucose and insulin remained constant (Figures S1A and S1B). The
162 transcriptomic data were reported in our previous studies (Egami et al., 2021; Kokaji et
163 al., 2020), and the metabolomic and proteomic data were newly obtained in this study
164 (Materials and Methods). We selected 28 metabolites, 15 proteins and 17 transcripts in
165 the glucose metabolism from the metabolomic, proteomic and transcriptomic data (Table
166 S2). Principal component analysis of the metabolites, proteins and transcripts showed that
167 the first principal components captured differences between WT and *ob*/*ob* mice, and the
168 second principal components captured changes by oral glucose administration (Figure
169 S1C). For the metabolites, proteins and transcripts, the explained variance ratio of the
170 first principal components (58%, 81% and 50%) exceeded 50%, and the second principal
171 components (11%, 8% and 15%) were less than 15%. This result suggests that the
172 differences in the metabolites, proteins and transcripts in the glucose metabolism between
173 WT and *ob*/*ob* mice were larger than changes by oral glucose administration.
174 We defined increased and decreased molecules between the conditions.
175 Molecules that showed an FDR-adjusted p value (q value) less than 0.05 are defined as

176 significantly changed molecules. Among them, molecules that showed a fold change
177 larger than 1.5 and smaller than 0.67 were defined as increased and decreased molecules
178 between the conditions.

179 At fasting state, increased metabolites in *ob*/*ob* mice compared to WT mice
180 included those in glycogenolysis (glycogen and glucose 1-phosphate; G1P),
181 gluconeogenesis (glucose 6-phosphate; G6P, fructose 6-phosphate; F6P, fructose 1,6-
182 bisphosphate; F1,6P and phosphoenolpyruvate; PEP) and TCA cycle (citrate and
183 succinate). Decreased metabolites in *ob*/*ob* mice included lactate and acetyl-CoA. After
184 oral glucose administration, increased metabolites in *ob*/*ob* mice compared to WT mice
185 were similar to those at fasting state except for a few metabolites (glycogen, glycerol 3-
186 phosphate; G3P, PEP, malate, alanine and acetyl-CoA), which did not significantly
187 change between WT and *ob*/*ob* mice. Metabolites that significantly increased by glucose
188 administration in WT mice included those in glycogenolysis (glycogen and G1P) and
189 gluconeogenesis (G6P, F6P and PEP). In contrast, in *ob*/*ob* mice no metabolites in the
190 glucose metabolism were significantly changed by glucose administration.

191 We identified increased and decreased proteins between the conditions. At
192 fasting state, increased proteins in *ob*/*ob* mice compared to WT mice included those in
193 gluconeogenesis (glucose-6-phosphate isomerase 1; Gpi1, fructose bisphosphatase 1;
194 Fbp1, glycerol-3-phosphate dehydrogenase 1; Gpd1, phosphoglycerate mutase 1; Pgam1
195 and enolase 1; Eno1), lactate dehydrogenase A (Ldha) and pyruvate kinase (Pklr).
196 Phosphoenolpyruvate carboxykinase 1 (Pck1) was the only protein in the glucose
197 metabolism that decreased in *ob*/*ob* mice. After oral glucose administration, increased
198 proteins in *ob*/*ob* mice compared to WT mice included those in gluconeogenesis (Gpi1,
199 Fbp1 and Gpd1) and Pklr. No proteins increased or decreased by oral glucose
200 administration in WT or *ob*/*ob* mice.

201 We identified increased and decreased transcripts between the conditions. At
202 fasting state, increased transcripts in *ob*/*ob* mice compared to WT mice included *Gpd1*

and *Pklr*. After oral glucose administration, increased transcripts in *ob*/*ob* mice included *Gpi1*, *Pklr* and *Cs*. No transcripts increased or decreased by glucose administration in WT or *ob*/*ob* mice.

The amounts of metabolites, proteins and transcripts do not directly reflect metabolic flux and its regulation; however, these data contain sufficient information to infer metabolic flux and its regulation. Therefore, we developed a method to infer metabolic flux and its regulation using the metabolomic, proteomic and transcriptomic data.

Inference of metabolic fluxes by OMELET

We developed a method that we term OMELET to infer metabolic fluxes in the glucose metabolism in each condition, and to identify changes in metabolic flux between the conditions (Figures 3 and S2). Briefly, OMELET evaluated the likelihoods of the enzymes and transcripts using kinetic equations combined with prior and hyperprior for metabolic flux under steady-state assumption. Because the blood glucose and insulin remained constant both in WT and *ob*/*ob* mice at fasting state and four hours after oral glucose administration (Figures S1A and S1B), we assumed steady-state conditions for the glucose metabolism in livers of WT and *ob*/*ob* mice.

The inputs of OMELET are the experimental data of the amounts of metabolites $\boldsymbol{x}$, proteins $\boldsymbol{e}$ and transcripts $\boldsymbol{t}$ from the same individual mice in each condition as well as model definitions including stoichiometric matrix and information on cofactors and allosteric effectors. The outputs are metabolic fluxes in the glucose metabolism $\boldsymbol{v}'$ in each condition, elasticity coefficients $\boldsymbol{\epsilon}$ and protein turnover coefficients $\boldsymbol{\beta}$. OMELET was based on a Bayesian method calculating posterior probability of the output parameters $p(\boldsymbol{v}', \boldsymbol{\epsilon}, \boldsymbol{\beta} | \boldsymbol{x}, \boldsymbol{e}, \boldsymbol{t})$ by updating prior probability of parameters ($p(\boldsymbol{v}' | \boldsymbol{u})$, $p(\boldsymbol{\epsilon})$ and $p(\boldsymbol{\beta})$) and hyperprior of independent flux $p(\boldsymbol{u} | \boldsymbol{\mu}^u)$ through evaluating likelihoods of the proteomic and transcriptomic data under a given parameter set

230 $p(\boldsymbol{e}, \boldsymbol{t}|\boldsymbol{x}, \boldsymbol{v}', \boldsymbol{\beta}, \boldsymbol{\epsilon})$ (Materials and Methods). We used the elasticity coefficients $\boldsymbol{\epsilon}$ and
231 protein turnover coefficients $\boldsymbol{\beta}$ simultaneously inferred with metabolic fluxes $\boldsymbol{v}'$ to
232 calculate contributions of regulators to the changes in metabolic flux between the
233 conditions. OMELET allowed us to identify changes in metabolic flux between the
234 conditions as well as the extent to which regulators such as changes in the amounts of
235 enzymes and metabolites contributed the changes in metabolic flux between the
236 conditions.

237 We validated the performance of OMELET by applying it to the simulated
238 datasets of the amounts of metabolites, enzymes and metabolic fluxes in five conditions
239 from a kinetic model expressing yeast glycolysis (Messiha et al., 2014; Smallbone et al.,
240 2013) (Figure S3; Table S3). The metabolic fluxes inferred by OMELET showed high
241 correlation with those generated by steady-state simulation of the kinetic model (Figure
242 S3), indicating that OMELET accurately identify the difference of metabolic fluxes across
243 reactions in the glycolysis in each condition and changes in metabolic flux among
244 conditions.

245

246 **Inference of metabolic fluxes in the glucose metabolism in liver of WT and *ob*/*ob***
247 **mice at fasting state and after oral glucose administration**

248 By applying OMELET to the experimental data, we inferred metabolic fluxes in the
249 glucose metabolism in four conditions of WT and *ob*/*ob* mice at fasting state and after
250 oral glucose administration (Figure 4A; Table S4). The posterior distributions of the
251 metabolic fluxes were obtained by fitting the model to the experimental data of the
252 amounts of enzymes and transcripts in each condition (Figure S4). We assumed that
253 glucose production was dominant in all the conditions analyzed according to the previous
254 studies (Jin et al., 2013; Turner et al., 2005), and fixed the direction of the metabolic flux
255 from G6P to glucose, which we called glucose-6-phosphatase (G6PC) in this study, as
256 glucose production. A metabolic flux through each reaction was simultaneously inferred

257 in all the conditions relative to that through G6PC in WT mice at fasting state (Materials
258 and Methods).

259 The metabolic flux through G6PC as glucose production is the sum of that
260 through phosphoglucomutase (PGM) in glycogenolysis and fructose-1,6-bisphosphatase
261 (FBPase) in gluconeogenesis. In WT mice at fasting state, the median of metabolic flux
262 through FBPase (0.92) was larger than that through PGM (0.17), suggesting that glucose
263 production was dependent on gluconeogenesis (Figure 4A: WT at fasting state). The small
264 metabolic flux through PGM is consistent with the depletion of glycogen in WT mice at
265 fasting state (Figure 2). The metabolic flux through FBPase was further divided into that
266 through glycerol-3-phosphate dehydrogenase (GPD) and alpha-enolase (ENO), which
267 represented the metabolic flux through gluconeogenesis from glycerol and PEP,
268 respectively. The median of metabolic flux through ENO (1.1) was larger than that
269 through GPD (0.75), indicating that PEP is preferentially used for glucose production
270 compared to glycerol. In pyruvate cycle, the median of metabolic flux through PEPCK
271 (2.1) and pyruvate carboxylase (PC, 1.8) was larger than that through ENO (1.1), while
272 that through PK (0.98) was smaller. This result suggests that PEP was preferentially used
273 for glucose production rather than returning to pyruvate. The median of metabolic flux
274 through PK (0.98) was larger than those through alanine aminotransferase (GPT, 0.41)
275 and lactate dehydrogenase (LDH, 0.35), suggesting that the return of PEP to pyruvate
276 through PK was the major source for pyruvate. In TCA cycle, 95% credible intervals of
277 the metabolic fluxes were large, indicating that the metabolic fluxes through reactions in
278 TCA cycle were not reliably determined. The metabolic fluxes in the glucose metabolism
279 in liver of fasting WT mice inferred by OMELET were consistent with those in the
280 previous metabolic flux analyses in fasting WT mice (Burgess et al., 2015; Hasenour et
281 al., 2015, 2020; Satapati et al., 2012; Wang et al., 2020) (Figures S5A and S5B), indicating
282 that OMELET was sufficiently accurate to infer the metabolic fluxes in the glucose
283 metabolism in liver of WT mice at fasting state.

284 For *ob*/*ob* mice at fasting state, we calculated fold changes of the metabolic flux
285 of *ob*/*ob* mice over that of WT mice for each reaction (Figure 4B (i)). The medians of fold
286 changes of metabolic fluxes through FBPase (2.01), GPD (2.47), ENO (1.74) in
287 gluconeogenesis, LDH (2.50), GPT (2.24) in lactate and alanine metabolism, PK (1.59),
288 PC (2.04) and PEPCK (2.24) in pyruvate cycle were larger than those through reactions
289 in glycogenolysis and TCA cycle. The metabolic flux through G6PC, glucose production,
290 is a sum of the metabolic flux through PGM, GPD, LDH, GPT and glutamate
291 dehydrogenase (GLUD). We quantified the fraction of sources of the glucose production
292 by calculating the proportion of the metabolic flux through PGM, GPD, LDH, GPT and
293 GLUD to that through G6PC, which represent glycogen, glycerol, lactate, alanine and
294 glutamate as sources, respectively (Figure 4C). The fraction of glycerol increased from
295 34% in fasting WT mice to 45% in fasting *ob*/*ob* mice, suggesting that fat accumulation
296 in liver of *ob*/*ob* mice caused an increased supply of glycerol as a precursor for glucose.
297 The fraction of alanine increased from 19% in fasting WT mice to 24% in fasting *ob*/*ob*
298 mice while that of lactate decreased from 16% to 13%, implying the increased glucose-
299 alanine cycle and decreased glucose-lactate cycle in *ob*/*ob* mice. To evaluate the
300 efficiency to utilize carbons of PEP for glucose production through gluconeogenesis
301 rather than for returning to pyruvate through pyruvate cycle, we compared the
302 composition of the metabolic flux through PEPCK between fasting WT and *ob*/*ob* mice
303 (Figure 4D). Compared to WT mice, the composition of the metabolic flux through PK
304 in *ob*/*ob* mice increased and was comparable with the composition of that through ENO,
305 indicating the less efficient use of PEP as a source of glucose in *ob*/*ob* than in WT mice.
306 The fold changes of the metabolic fluxes through most reactions in the glucose
307 metabolism of *ob*/*ob* mice over that of WT mice inferred by OMELET were consistent
308 with those in the previous metabolic flux analyses in fasting *ob*/*ob* mice (Turner et al.,
309 2005) and high-fat diet-induced obese mice (Patterson et al., 2016; Satapati et al., 2012)
310 except for that through glycogenolysis (Figures S5C and S5D). Collectively, we identified

311 increases in metabolic fluxes through gluconeogenesis and pyruvate cycle in *ob*/*ob* mice
312 compared to WT mice at fasting state.
313 For metabolic fluxes after oral glucose administration, we calculated fold
314 changes of the metabolic flux after oral glucose administration over that at fasting state
315 in WT and *ob*/*ob* mice (Figures 4B (iii) and (iv)). The metabolic fluxes through most
316 reactions slightly increased in WT mice and decreased in *ob*/*ob* mice by oral glucose
317 administration. As an exception, the metabolic flux through PK slightly decreased by oral
318 glucose administration both in WT and *ob*/*ob* mice. Changes in the sources of glucose
319 production and the composition of the metabolic flux through PEPCK by oral glucose
320 administration were smaller than those between WT and *ob*/*ob* mice (Figures 4C and 4D).
321 These results suggest the change in metabolic flux between WT and *ob*/*ob* mice at fasting
322 state was maintained after oral glucose administration while metabolic fluxes slightly
323 increased in WT mice and decreased in *ob*/*ob* mice by oral glucose administration.
324
325 **Contributions of regulators to changes in metabolic flux between fasting WT and**
326 ***ob*/*ob* mice**
327 A metabolic flux is controlled by multiple regulators including enzymes, substrates,
328 products, cofactors and allosteric effectors. To investigate which regulator caused
329 changed metabolic flux between the conditions, we quantified contributions of the
330 regulators to changes in metabolic flux between the conditions (Figures 5 and S6 (i);
331 Table S5). For each regulator, we calculated the product of the squared sensitivity of the
332 regulator to metabolic flux, which is calculated using the elasticity coefficients (Figure
333 S7) and turnover coefficients, and the squared change in the amounts of the regulator
334 between the conditions. The contribution of the regulator is defined as the proportion of
335 the product of the regulator to the sum of the products of all the regulators following the
336 method previously described (Hackett et al., 2016) (Materials and Methods).
337 We defined contributions of regulators to changes in metabolic flux (Figure 5A).

338 The regulators of metabolic flux were transcripts, unaccounted enzyme regulators,
339 substrates, products, cofactors, allosteric effectors and unaccounted flux regulators. The
340 unaccounted 'enzyme' regulators can include other regulatory mechanisms of the protein
341 amount of enzyme such as protein degradation and stability. The unaccounted 'flux'
342 regulators can include other regulatory mechanisms of the metabolic flux such as
343 phosphorylation of enzymes and unknown allosteric effectors which were not included in
344 OMELET. The contribution of regulator h to a change in metabolic flux through each
345 reaction ψ_h was calculated as

$$\psi_h = \frac{\left(\frac{\partial v}{\partial y_h}\right)^2 (\Delta y_h)^2}{\sum_h \left(\frac{\partial v}{\partial y_h}\right)^2 (\Delta y_h)^2}$$

346 with a sensitivity of the regulator to the metabolic flux v $(\partial v/\partial y_h)$ and a change in the
347 amount of the regulator between conditions Δy_h. The contribution is calculated for
348 changes in metabolic flux through each reaction between each pair of condition. The sum
349 of the contributions of all regulators to a change in metabolic flux equals one, and a larger
350 contribution indicates a stronger regulatory effect on metabolic flux. We discussed
351 regulators whose contributions were larger than 0.25 below.

352 The contribution is represented as a distribution (Figure S6 (i)), and the mean of
353 the distribution is shown in the same order of regulators (Figure 5B). The contribution is
354 a normalized value for each metabolic flux and independent of the magnitude of the
355 changes in metabolic flux between the conditions. We examined the relationships between
356 the contributions of enzyme or metabolite and the fold changes of the metabolic flux of
357 *ob*/*ob* mice over that of WT mice at fasting state (Figures 5C and 5D). The contribution
358 of enzyme is the sum of that of transcript and unaccounted enzyme regulators, and the
359 contribution of metabolites is the sum of that of substrate, product, cofactor and allosteric
360 effector.

361 For the contribution of enzyme, the larger contributions of enzyme showed the

362 larger fold changes of the metabolic flux (Figure 5C). By contrast, for the contribution of
363 metabolite, the smaller contributions of metabolite showed the smaller fold changes of
364 the metabolic flux (Figure 5D). Exceptionally, for PEPCK, the contribution of enzyme
365 was smaller, and that of metabolite was larger.

366 The contribution of a regulator is functionally effective only when the fold
367 change of metabolic flux is large. We assumed that fold change of metabolic flux more
368 than 1.5 is important, and further investigated the contributions of regulators for such
369 metabolic flux (Figure 5B, red). Such metabolic fluxes included those through reactions
370 in gluconeogenesis, lactate and alanine metabolism, and pyruvate cycle, but not in
371 glycogenolysis or TCA cycle. In most reactions, the contribution of transcript was largest
372 among regulators, indicating that the increased metabolic fluxes were mainly caused by
373 increased transcripts. Exceptionally, for PEPCK, that of substrate (0.74) was larger,
374 indicating that increased metabolic flux through PEPCK in pyruvate cycle was caused by
375 increased substrates.

376

377 **Quantitative trans-omic networks for changes in metabolic flux between WT and**
378 ***ob*/*ob* mice at fasting state**

379 To reveal a global landscape of alteration and dysregulation of metabolic flux in fasting
380 *ob*/*ob* mice, we constructed a quantitative trans-omic network by integrating the
381 experimental data (Figure 2), the changes in metabolic flux (Figure 4), and the
382 contributions of the regulators (Figure 5) (Figure 6). The quantitative trans-omic network
383 consisted of four layers (Transcript, Enzyme, Metabolic Flux and Metabolite) (Figures
384 6A-D). Nodes in Transcript, Enzyme and Metabolite layer (circles) represented the
385 transcripts, proteins and metabolites. Nodes in Metabolic Flux layer (lines within layer)
386 represented the reactions. Edges from Transcript layer to Enzyme layer represented
387 regulation of enzyme by transcript, and those by unaccounted enzyme regulators were not
388 displayed. Edges from Enzyme layer to Metabolic Flux layer represented contributions

389 of enzyme to changes in metabolic flux between the conditions. Edges from Metabolite
390 layer to Metabolic Flux layer represent regulation of changes in metabolic flux by
391 metabolites as substrate, product, cofactor and allosteric effector. Unaccounted flux
392 regulators were not displayed. The size of nodes represents fold changes of corresponding
393 molecules of *ob*/*ob* mice over those of WT mice, and the size of edges represents
394 contributions of regulators to changes in metabolic flux.

395 We extracted the subnetwork of gluconeogenesis and lactate and alanine
396 metabolism (Figure 6C), and pyruvate cycle (Figure 6D), where the fold-change of
397 metabolic flux is larger than 1.5 (Figure 5B, red). In the subnetwork of gluconeogenesis
398 and lactate and alanine metabolism (Figure 6C), enzymes including Gpi1, Fbp1, Gpd1,
399 Pgam1, Eno1, Ldha in Enzyme layer as well as substrates and products including G6P,
400 F6P, F1,6P, PEP and alanine in Metabolite layer increased in *ob*/*ob* mice. The edges from
401 the enzymes in Enzyme layer to reactions including glucose-6-phosphate isomerase (GPI),
402 FBPase, GPD, phosphoglycerate mutase (PGAM), ENO, LDH and GPT in Metabolic
403 Flux layer (0.89-0.98) were larger than those from the metabolites in Metabolite layer to
404 the reactions in Metabolic Flux layer (less than 0.10), indicating that the contributions of
405 enzyme were larger than those of metabolites. The edges from transcripts including *Gpd1*,
406 *Pgam1*, *Eno1*, *Ldha* and *Gpt* in Transcript layer to the enzymes in Enzyme layer were
407 almost equal to those from the enzymes in Enzyme layer to the reactions in Metabolic
408 Flux layer except for Gpi1 (0.50 and 0.90) and Fbp1 (0.15 and 0.96), indicating that
409 contributions of enzyme to changes in metabolic flux were explained by those of
410 transcript in most of the reactions. These results indicate that the increased gene
411 expression of enzymes mainly contributed to the increased metabolic fluxes, which
412 caused increased metabolites in gluconeogenesis and lactate and alanine metabolism in
413 *ob*/*ob* mice (Figure 6E).

414 In the subnetwork of pyruvate cycle (Figure 6D), substrates including PEP,
415 pyruvate and oxaloacetate in Metabolite layer connected to PK, PC and PEPCK in

416 Metabolic Flux layer increased in *ob*/*ob* mice. In contrast, Pklr in Enzyme layer connected
417 to PK in Metabolic Flux layer increased, pyruvate carboxylase (Pcx) connected to PC was
418 not significantly changed, and Pck1 connected to PEPCK decreased in *ob*/*ob* mice. The
419 edge from Pklr in Enzyme layer to PK in Metabolic Flux layer (0.86) was larger than
420 edges from its substrate PEP in Metabolite layer to PK in Metabolic Flux layer (0.12),
421 indicating that enzyme, rather than metabolite, contributed to changes in metabolic flux
422 through PK. The edge from Pcx in Enzyme layer to PC in Metabolic Flux layer (0.61)
423 and that from its substrate pyruvate in Metabolite layer to PC in Metabolic Flux layer
424 (0.31) were large, indicating that both enzyme and substrate contributed to changes in
425 metabolic flux through PC. The edge from Pck1 in Enzyme layer to PEPCK in Metabolic
426 Flux layer (0.18) was smaller than that from its substrate oxaloacetate in Metabolite layer
427 to PEPCK in Metabolic Flux layer (0.74), indicating that substrate, rather than enzyme,
428 contributed to changes in metabolic flux through PEPCK. In all metabolic fluxes through
429 PK, PC and PEPCK in pyruvate cycle, edges from *Pklr*, *Pcx* and *Pck1* in Transcript layer
430 to Pklr, Pcx and Pck1 in Enzyme layer (0.86, 0.59 and 0.18) were almost equal to those
431 from Pklr, Pcx and Pck1 in Enzyme layer to PK, PC and PEPCK in Metabolic Flux layer
432 (0.86, 0.61 and 0.18), indicating that the contributions of enzyme to changes in the
433 metabolic flux were explained by those of transcript. Collectively, the main regulator of
434 changes in metabolic flux between WT and *ob*/*ob* mice was an increased transcript for
435 the metabolic flux through PK, an increased transcript and substrate for that through PC,
436 and an increased substrate for that through PEPCK (Figure 6E). These results suggest that
437 the increased *Pklr* expression triggered the increased metabolic flux through pyruvate
438 cycle, which caused the accumulations of substrates including pyruvate and oxaloacetate,
439 and large contributions of substrates to increases in metabolic fluxes through downstream
440 reactions of PC and PEPCK.

441 We also constructed a quantitative trans-omic network after oral glucose
442 administration (Figure S8), which showed similar features with those at fasting state. This

443 result indicates that oral glucose administration had little effect on changes in the
444 metabolic flux between WT and *ob*/*ob* mice, and the contributions of the regulators to the
445 changes in the metabolic flux.
446
447 **Contributions of regulators to changes in metabolic flux by oral glucose**
448 **administration**
449 We quantified contributions of the regulators to changes in metabolic flux by oral glucose
450 administration in WT and *ob*/*ob* mice (Figures 7, S6 (iii) and (iv);Table S5). We examined
451 the relationships between contributions of enzyme or metabolite to changes in metabolic
452 flux and fold changes of metabolic fluxes after oral glucose administration over those at
453 fasting state (Figure 7A). None of the reactions showed a fold change of metabolic flux
454 more than 1.5 nor less than 0.67, and no apparent relationship was found between the
455 contributions of enzyme or metabolite and fold changes of the metabolic flux by oral
456 glucose administration.
457 Among all the reactions, the biggest difference in the contribution of the
458 regulators by oral glucose administration between WT and *ob*/*ob* mice was found in PK
459 (Figure 7B, right). The contribution of allosteric effectors to the change in metabolic flux
460 through PK was the largest in WT mice (0.55, Figures 7B (iii) and S6 (iii)), whereas the
461 contribution of transcript was the largest in *ob*/*ob* mice (0.93). These results suggest that
462 the change in metabolic flux through PK by oral glucose administration was caused by
463 different mechanisms between WT and *ob*/*ob* mice: changed allosteric effectors in WT
464 mice and changed transcripts in *ob*/*ob* mice.
465 To explore the differences of the contributions of the regulators to the decreased
466 metabolic flux through PK between WT and *ob*/*ob* mice, we constructed a quantitative
467 trans-omic network for the change metabolic flux through PK by oral glucose
468 administration in WT mice (Figure 7C (iii)) and *ob*/*ob* mice (Figure 7C (iv)). In WT mice,
469 the substrate PEP and allosteric inhibitor ATP in Metabolite layer increased by oral

470 glucose administration (Figure 7C (iii)). The edge from ATP in Metabolite layer to PK in
471 Metabolic Flux layer (0.50) was the largest among the edges from the metabolites in
472 Metabolite layer to PK in Metabolic Flux layer, indicating that the contribution of ATP
473 was the largest among the metabolites. In *ob*/*ob* mice, no metabolites in Metabolite layer
474 increased nor decreased by oral glucose administration (Figure 7C (iv)). The edge from
475 Pklr in Enzyme layer to PK in Metabolic Flux layer (0.95) was larger than edges from the
476 metabolites including PEP, ADP, F1,6P, ATP, alanine and phenylalanine in Metabolite
477 layer to PK in Metabolic Flux layer (less than 0.10), indicating that the contribution of
478 enzyme was larger than that of the metabolites. The edge from *Pklr* in Transcript layer to
479 Pklr in Enzyme layer (0.93) was almost equal to that from Pklr in Enzyme layer to PK in
480 Metabolic Flux layer (0.95), indicating that the contribution of enzyme was explained by
481 those of transcript. These results suggest that the change in metabolic flux through PK
482 was caused by increased ATP as an allosteric inhibitor in WT mice and by slightly
483 decreased *Pklr* transcript in *ob*/*ob* mice. Given that the changes of metabolic flux through
484 PK was not large by oral glucose administration (Fig. 4B), WT and *ob*/*ob* mice used
485 different regulatory mechanisms, allosteric regulation and transcripts, respectively, to
486 maintain the metabolic flux through PK rather than to change metabolic flux.

DISCUSSION

In this study, we developed a method OMELET to investigate alterations and dysregulation of metabolic flux in liver associated with obesity. Using OMELET, we inferred metabolic fluxes in the glucose metabolism in livers of WT and *ob*/*ob* mice at fasting state and after oral glucose administration to identify changes in metabolic flux between the conditions. The metabolic flux through reactions in gluconeogenesis and pyruvate cycle increased in *ob*/*ob* mice compared to WT mice at fasting state. The increased metabolic fluxes through reactions in gluconeogenesis were mainly caused by increased transcripts. In contrast, the increased metabolic fluxes through PK and PEPCK in pyruvate cycle were caused by increased transcript and substrate, respectively. By oral glucose administration, changes in metabolic fluxes were small compared to those between WT and *ob*/*ob* mice. In WT mice, slightly decreased metabolic flux through PK by oral glucose administration was caused by increased ATP as an allosteric inhibitor, whereas in *ob*/*ob* mice the slightly decreased PK flux was caused by the slightly decreased transcript. Given that the changes in metabolic flux through PK was not large by oral glucose administration (Figure 4B), WT and *ob*/*ob* mice used different regulatory mechanisms, allosteric regulation and transcripts, respectively, to maintain the metabolic flux through PK rather than to change metabolic flux.

Although an isotopic labeling experiment is a powerful technique to measure metabolic flux, the addition of isotopic tracers introduced into living animals may perturb the activity of the metabolic pathway of interest. OMELET does not require isotopic labeling data to infer metabolic flux, and can avoid possible perturbations caused by the addition of isotopic tracers. However, the accuracy of inference of metabolic flux without isotopic labeling data is needed to be validated. We validated the performance of OMELET by applying it to the simulated datasets from a kinetic model expressing the yeast glycolysis (Messiha et al., 2014; Smallbone et al., 2013) (Figure S3). We also applied OMELET to the data in fasting mouse liver and found that the inferred metabolic

514 fluxes in WT mice were consistent with those in the previous studies (Figures S5A and
515 S5B). The fold changes of the metabolic fluxes through most reactions in the glucose
516 metabolism of *ob*/*ob* mice over that of WT mice inferred by OMELET were consistent
517 with those in the previous studies, except for that through glycogenolysis (Figures S5C
518 and S5D). These results suggest that the experimental data of the amounts of enzymes
519 and metabolites contain information on metabolic fluxes as latent parameters, which can
520 be inferred by a generative model in OMELET.

521 We used the simultaneously obtained experimental dataset of the amounts of
522 metabolites, proteins and transcripts of the same samples for OMELET. Such datasets
523 enabled us to apply a Bayesian method rather than analyzing the population mean. A
524 Bayesian method can incorporate uncertainties inherent in the experimental data, such as
525 measurement noise and population heterogeneity. Based on a Bayesian method, we
526 assume the experimental data to have arisen from a generative model describing the
527 underlying processes given latent parameters and evaluate the probability that the model
528 yields the data by likelihood. In OMELET, the enzymes were derived from a generative
529 model based on metabolic flux, and the transcripts from a generative model based on
530 protein turnover (Figures 3 and S2). Using these two generative models in OMELET, we
531 evaluated the likelihood of the enzymes and transcripts from each mouse to infer
532 unknown parameters including metabolic fluxes, elasticity coefficients and protein
533 turnover coefficients. Using simultaneously obtained multi-omic data, although it is not
534 easy to obtain such data because of experimental and technical costs, a Bayesian method
535 has the potential to analyze metabolic flux (Heinonen et al., 2019) and its regulation
536 (Hackett et al., 2016; John et al., 2019; Saa and Nielsen, 2016).

537 There are several limitations in this study. The 95% credible intervals of the
538 metabolic fluxes in TCA cycle were large, indicating that the metabolic fluxes in TCA
539 cycle were not reliably determined (Figure 4A). The inaccuracy of the inferred metabolic
540 fluxes in TCA cycle may be due to little changes in the amounts of enzymes and

541 metabolites in TCA cycle between the conditions. We do not consider the
542 compartmentation of reactions into cytoplasm and mitochondria, and inferred metabolic
543 fluxes averaged in a whole cell, which may result in the inaccuracy of inference of
544 metabolic fluxes. In addition, OMELET is based on a steady-state assumption and cannot
545 infer dynamic changes in metabolic flux under non-steady-state conditions.

546 Using OMELET, we found alteration and dysregulation of metabolic flux
547 associated with obesity. We found that the large increase in metabolic flux through
548 reactions in gluconeogenesis and lactate and alanine metabolism in *ob*/*ob* mice compared
549 to WT mice at fasting state was mainly caused by increased gene expression of the
550 enzymes (Figure 4). There are several transcription factors involved in the control of gene
551 expressions in gluconeogenesis and lactate and alanine metabolism. For example, CREB
552 (cAMP response element-binding protein) activates transcription of *G6pc* and *Fbp1*
553 (Hanson and Reshef, 1997; Herzig et al., 2001), as well as *Gpi1*, *Pgam1*, *Ldha* and *Gpt*
554 (Everett et al., 2013). Liver-specific knockdown of CREB reduced fasting plasma glucose
555 concentrations in *ob*/*ob* mice through downregulation of *G6pc* and *Fbp1* (Erion et al.,
556 2009). In addition to these key transcription factors identified by individual experiments,
557 the recent high-throughput measurements and multi-omic analysis have revealed many
558 more transcription factors responsible for metabolic alteration associated with obesity
559 (Egami et al., 2021; Kokaji et al., 2020; Soltis et al., 2017). These studies suggest that
560 transcription factors contribute changes in metabolic flux in glucose metabolism
561 associated with obesity, but metabolic flux is also regulated by metabolites including
562 substrates, products, cofactors and allosteric effectors. In this study, we found that
563 transcripts, rather than metabolites, mainly contributed to the changes in metabolic flux
564 (Figure 4). Our results suggest that transcription factors would trigger increased
565 gluconeogenic flux associated with obesity by modulating gene expression of the
566 enzymes.

567 In pyruvate cycle, increased oxaloacetate as substrate, rather than Pck1 amount,

568 contributed increased metabolic flux through PEPCK in fasting *ob*/*ob* mice (Figure 5B).
569 Several metabolic flux analyses showed that the metabolic flux through PEPCK increased
570 associated with obesity (Patterson et al., 2016; Satapati et al., 2012; Sunny et al., 2011),
571 which was consistent with our result (Figure 4B). Given that PEPCK is an irreversible
572 reaction and there are no known allosteric effectors, possible regulators of the metabolic
573 flux through PEPCK include Pck1 amounts, oxaloacetate as substrate, and GTP as
574 cofactor. However, it has been unclear which regulator mainly contributed the increased
575 metabolic flux through PEPCK associated with obesity. Among the possible regulators,
576 Pck1 amounts decreased associated with obesity at fasting state (Samuel et al., 2009;
577 Satapati et al., 2012; Sunny et al., 2011), which was observed in our proteomic data
578 (Figure 2). These studies suggest that the increased metabolic flux through PEPCK
579 associated with obesity at fasting state is not consistent with the decreased Pck1 amount.
580 Here we found that increased oxaloacetate, rather than Pck1 and GTP, contributed the
581 increased metabolic flux through PEPCK (Figure 5B). Therefore, the increased metabolic
582 flux through PEPCK associated with obesity can be explained by increased oxaloacetate.
583 The difference in contributions of regulators by oral glucose administration
584 between WT and *ob*/*ob* mice was found only in the changes in metabolic flux through PK.
585 In WT mice, the contribution of allosteric effectors, especially of ATP, was the largest
586 among regulators of metabolic flux through PK, while in *ob*/*ob* mice that of transcript
587 was the largest. The reason why allosteric regulation was not the main regulator in *ob*/*ob*
588 mice may be because amounts of allosteric effectors such as ATP are high even at fasting
589 state and do not increase by oral glucose administration (Figure 2).
590 In calculating contributions of regulators to changes in metabolic flux between
591 the conditions, we considered unaccounted flux regulators as one of the regulators of
592 metabolic flux and unaccounted enzyme regulators as one of the regulators of enzymes.
593 The contributions of unaccounted flux regulators to changes in metabolic flux between
594 fasting WT and *ob*/*ob* mice were smaller than those of other regulators in all the reactions

595 in gluconeogenesis and pyruvate cycle, indicating that changes in metabolic fluxes
596 through these reactions can be explained by known regulators (Figures 5C and S6 (i)). In
597 contrast, the contributions of unaccounted enzyme regulators to changes in enzyme in
598 reactions through GPI and FBPase were relatively larger than those through other
599 reactions, indicating that the increase in enzyme in *ob*/*ob* mice cannot be explained by
600 the transcripts. Although we used a simple linear relationship between the amount of a
601 protein and a transcript in OMELET, the increase in protein not accompanied by the
602 changes in transcripts should be explained by other regulatory mechanisms such as
603 protein degradation and stability. Furthermore, the contributions of unaccounted flux
604 regulators to changes in metabolic flux between fasting and after oral glucose
605 administration were larger in many reactions than those between fasting WT and *ob*/*ob*
606 mice (Figures. 6B, S6 (iii) and (iv)). To explain the contributions of unaccounted flux
607 regulators, we need to consider posttranslational modifications of enzymes such as
608 phosphorylation by including phosphoproteomic data.

609 In conclusion, we developed OMELET using the simultaneously obtained multi-
610 omic data to infer metabolic fluxes in the glucose metabolism in each condition, and to
611 identify changes in metabolic flux between the conditions. Furthermore, we quantified
612 contributions of the regulators to the changes in metabolic flux between the conditions.
613 OMELET is designed to infer metabolic flux without using isotopic labeling data, and to
614 simultaneously infer changes in metabolic flux and contributions of regulators. The
615 quantitative trans-omic network sheds light on the insights into the obesity-associated
616 changes in the glucose metabolism in liver, and provides comprehensive molecular
617 mechanisms for understanding the pathology of alteration and dysregulation of metabolic
618 flux associated with obesity.

ACKNOWLEDGEMENTS

We are grateful to Maki Ohishi, Ayano Ueno, Keiko Endo, Sanae Ashitani, Keiko Kato, and Kaori Saitoh (Keio University) for their technical assistance with metabolomic analysis using CE-MS. We thank for Shinsuke Uda and our laboratory members for critically reading this manuscript and for their technical assistance with the experiments. The computational analysis of this work was performed in part with support of the super computer system of National Institute of Genetics (NIG), Research Organization of Information and Systems (ROIS).

This work was supported by the Japan Society for the Promotion of Science (JSPS) KAKENHI Grant Number JP17H06300, JP17H06299, JP18H03979, JP21H04759 and by The Uehara Memorial Foundation. S.U. receives funding from JSPS KAKENHI Grant Number JP19J22134. S.O. receives funding from a Grant-in-Aid for Early-Career Scientists (JP17K14864 and JP21K14467). A. Hatano is supported by Grant-in Aid from the Tokyo Biochemical Research Foundation. T.K. receives funding from JSPS KAKENHI Grant Number JP21K16349. H.K. was supported by JSPS KAKENHI JP20H03237. Y.S. was supported by the JSPS KAKENHI Grant Number JP17H06306. K.I.N. was supported by the JSPS KAKENHI Grant Number JP17H06301, JP18H05215. A. Hirayama was supported by the JSPS KAKENHI Grant Number JP18H04804. T.S. receives funding from the AMEDCREST from the Japan Agency for Medical Research and Development (AMED) under Grant Number JP18gm0710003.

AUTHOR CONTRIBUTIONS

S.U., S.O., and S.K. conceived the project; A. Hatano, T.K., Y.I., H.K., M.M., and K.I.N. designed and performed the animal experiments; A. Hirayama and T.S. performed metabolomic analysis using CE-MS; Y.S. performed transcriptomic analysis using RNA-seq; M.M. and K.I.N. performed proteomic analysis using LC-MS/MS; S.U., S.O., K.T., A. Hatano, T.K., Y.I., and K.H. analyzed the data; S.U., S.O., and K.T. performed mathematical modeling analyses. S.U., S.O., and S.K. wrote the manuscript. All authors read and approved the final manuscript.

DECLARATION OF INTERESTS

The authors declare no competing interests.

MATERIAL AND METHODS

RESOURCE AVAILABILITY

Lead Contact

Further information and requests for resources and reagents should be directed to and will be fulfilled by the Lead Contact, Shinya Kuroda (skuroda@bs.s.u-tokyo.ac.jp).

Materials Availability

This study did not generate new unique reagents.

Data and Code Availability

The datasets generated during this study are in the published article. The MATLAB and R code for OMELET are available at GitHub (https://github.com/usa0ri/OMELET). An image for Docker container that include RStan and R software to perform OMELET is available at DockerHub Registry (https://hub.docker.com/repository/docker/saori/rstan).

EXPERIMENTAL MODEL AND SUBJECT DETAILS

Animals

We used the mouse liver samples obtained simultaneously with those previously published (Egami et al., 2021; Kokaji et al., 2020). Briefly, 10-week-old male C57BL/6J wild-type and *ob*/*ob* mice (Japan SLC, Inc., Shizuoka, Japan) were overnight (16 hours) fasted or administrated 2 g/kg body weight of glucose orally after overnight fasting. The mice before or four-hour after glucose loading were sacrificed by cervical dislocation and the whole or left lobe of the liver was dissected and immediately frozen in liquid nitrogen. The frozen liver was pulverized with dry ice to a fine powder with a blender and separated into tubes for transcriptomic, proteomic, and metabolomic measurements. Note that all the omics data was simultaneously measured from the same individual mice. All the mouse experiments were performed according to protocols approved by the animal ethics

committee of The University of Tokyo.

We had mice under four conditions: WT mice at fasting state (n=11), *ob*/*ob* mice at fasting state (n=12), WT mice after oral glucose administration (n=12), and *ob*/*ob* mice after oral glucose administration (n=12). The metabolomic data of five samples in each condition were reported in our previous studies (Egami et al., 2021; Kokaji et al., 2020). We newly obtained the metabolomic data from all the samples in this study. The transcriptomic data from all the samples at fasting state and five after oral glucose administration were reported in our previous studies. We newly obtained the transcriptomic data from seven samples after oral glucose administration in this study.

METHOD DETAILS

Metabolic network for glucose metabolism in mice

A metabolic network for glucose metabolism in mice was constructed to infer metabolic fluxes and quantify the contributions of regulators to changes in metabolic flux between conditions. The network consists of 27 metabolites and 22 reactions (Table S1) in gluconeogenesis, glycogenolysis, lactate and alanine metabolism, and TCA cycle (Figure 1).

The liver produces glucose through the gluconeogenesis and consumes glucose through glycolysis. The gluconeogenesis in liver includes reactions catalyzed by glucose-6-phosphate (G6PC) and fructose-bisphosphatase 1 (FBPase), while the glycolysis includes reactions by glucokinase (GK) and phosphofructokinase (liver type) (PFKL). Assuming that the metabolic flux through GK and PFKL were negligible in livers of WT and *ob*/*ob* mice in all the conditions, we included G6PC and FBPase in the metabolic network but not included GK and PFKL. This is supported by several studies showing that the glucose production was more dominant than the glucose consumption in livers of overnight fasting WT mice (Burgess et al., 2005; Hasenour et al., 2015, 2020; Satapati et al., 2012; Wang et al., 2020) and *ob*/*ob* mice (Turner et al., 2005). In addition, the glucose

704 production from glycogenolysis and gluconeogenesis occurred 150 min after oral glucose
705 administration in rat (Jin et al., 2003). Although we did not find any studies to support the
706 glucose production in *ob*/*ob* mice four hours after oral glucose administration, *ob*/*ob* mice
707 after oral glucose administration in this study showed similar temporal changes in blood
708 glucose and insulin (Figures S1A and B) to WT mice. Therefore, we included G6PC and
709 FBPase in the metabolic network but not included GK and PFKL reactions. This also
710 reduces the complexity of the metabolic model and computational cost for the metabolic
711 flux estimation.

712 Pyruvate dehydrogenase (PDH), converting pyruvate to acetyl-CoA, was not
713 included in the metabolic network because several studies showed that the metabolic flux
714 through PDH was small (~5%) relative to those through TCA cycle in WT mice at fasting
715 state (Perry et al., 2016). Malic enzyme (ME), converting malate to pyruvate, was not
716 considered because ME inhibitor did not affect the metabolic flux producing pyruvate in
717 fasting rodent models (Hasenour et al., 2020; Perry et al., 2016; Petersen et al., 1995),
718 suggesting the small contribution of ME to the metabolic flux.

719 Cytoplasmic and mitochondrial compartments were not considered for
720 simplification and averaged metabolic fluxes as a single compartment were inferred in
721 this study. Malate dehydrogenase (Mdh) has cytoplasmic (Mdh1) and mitochondrial
722 (Mdh2) isoforms, but we only consider Mdh2 as a part of reactions in TCA cycle for
723 simplification.

724

725 **Algorithm of omics-based metabolic flux estimation without labeling for extended**
726 **trans-omic analysis (OMELET)**

727 We first review a framework of Bayesian inference. Statistical model consists of a
728 likelihood, representing a probability of the observed data $\boldsymbol{z}$ at a given parameter values
729 $\boldsymbol{\theta}$, and a prior distribution for $\boldsymbol{\theta}$, denoting a probability distribution of each parameter
730 reflecting the feasible assumptions and prior knowledges. Bayes' theorem calculates the

731 renormalized product of the likelihood $p(\boldsymbol{z}|\boldsymbol{\theta})$ and the prior distribution $p(\boldsymbol{\theta})$,

$$p(\boldsymbol{\theta}|\boldsymbol{z}) \propto p(\boldsymbol{z}|\boldsymbol{\theta})p(\boldsymbol{\theta})$$

732 to produce the posterior parameter distribution $p(\boldsymbol{\theta}|\boldsymbol{z})$, a probability of the parameters
733 taking the values given the observed data. The posterior distribution is obtained by
734 updating the parameter values following the prior distributions toward better fittings to
735 the observed data evaluated in likelihood. The definition of the prior distribution is critical
736 especially when the sample size is small whereas sufficient samples make its effects on
737 posterior parameter distribution decreases to get closer to maximal likelihood estimation.
738 One may assume additional parameters for prior distributions, which can be achieved by
739 defining hyperparameters $\boldsymbol{\eta}$,

$$p(\boldsymbol{\theta}, \boldsymbol{\eta}|\boldsymbol{z}) \propto p(\boldsymbol{z}|\boldsymbol{\theta})p(\boldsymbol{\theta}|\boldsymbol{\eta})p(\boldsymbol{\eta})$$

740 to introduce a hierarchical structure in prior distributions.

741 In Omics-based Metabolic flux Estimation without Labeling for Extended Trans-
742 omic analysis (OMELET), observed data $\boldsymbol{z}$ is the experimental data of the amounts of
743 metabolites, proteins and transcripts from the same samples obtained from multiple
744 conditions. The parameters $\boldsymbol{\theta}$ include metabolic fluxes in each condition, elasticity
745 coefficients in linlog kinetics and protein turnover coefficients. The prior $p(\boldsymbol{\theta})$ is
746 defined for all the parameters, and the hyperprior $p(\boldsymbol{\eta})$ is defined only for metabolic
747 fluxes, which has hyperparameters $\boldsymbol{\eta}$ to obtain a steady-state metabolic flux distribution
748 based on the reactions of the metabolic network of interest. The likelihood $p(\boldsymbol{z}|\boldsymbol{\theta})$, which
749 described the relationship between the experimental data and the parameters, is the
750 product of the probability of the measured amounts of enzymes given the parameters and
751 the probability of the measured amounts of transcripts given the parameters.

752

753 We start from defining the prior and hyperprior for metabolic fluxes as
754 multivariable normal distribution in each condition $l = 1,2,\ldots,g$. The metabolite
755 concentration $\boldsymbol{x}_l$ and metabolic fluxes $\boldsymbol{v}_l$ describes a system of mass balances around

each metabolite in the form

$$\dot{\boldsymbol{x}}_l = \boldsymbol{S}\boldsymbol{v}_l \tag{1}$$

for r reactions and m metabolites, where $\boldsymbol{S}$ denotes the stoichiometric matrix that links metabolites to their reactions via stoichiometry. Note that this stoichiometric matrix is based on the open-formed metabolic network that is transformed by removing rows for the metabolites that participated in transporting reaction across the system boundary, resulting in $m < r$. The vector of the time derivative for metabolites $\dot{\boldsymbol{x}}_l$ around steady state is assumed to follow m-dimensional multivariate normal distribution

$$\dot{\boldsymbol{x}}_l \sim \mathcal{N}\left(\boldsymbol{0}, \boldsymbol{\Sigma}_l^{\dot{x}}\right) \tag{2}$$

with diagonal covariance matrix $\boldsymbol{\Sigma}_l^{\dot{x}} = \mathrm{diag}\left(\left(\boldsymbol{\sigma}_l^{\dot{x}}\right)^\top \boldsymbol{\sigma}_l^{\dot{x}}\right)$. $\boldsymbol{\sigma}_l^{\dot{x}}$ represent the extent of relaxation from the steady state and are defined later based on the influx and efflux around each metabolite. The number of variables that need to be specified to calculate a steady-state fluxes in equation (1) is $f = r - \mathrm{rank}(\boldsymbol{S})$. Let us denote the vectors of independent and dependent flux variables $\boldsymbol{u}_l$ and $\boldsymbol{v}_j^d$ of length f and $\mathrm{rank}(\boldsymbol{S})$, respectively. Since dependent flux variables can be directly computed as linear combination of independent flux variables, we have only to estimate independent flux as hyperparameter to obtain the full metabolic fluxes. Here the vector of independent flux was assumed to follow the multi-dimensional normal distribution

$$p(\boldsymbol{u}_l|\boldsymbol{\mu}_l^u) = \mathcal{N}(\boldsymbol{u}_l|\boldsymbol{\mu}_l^u, \boldsymbol{\Sigma}_l^u) \tag{3}$$

with mean $\boldsymbol{\mu}_l^u$ and diagonal covariance matrix $\boldsymbol{\Sigma}_l^u = \mathrm{diag}((\boldsymbol{\sigma}_l^u)^\top \boldsymbol{\sigma}_l^u)$. The deviations of independent fluxes were determined as $\boldsymbol{\sigma}_l^u = c^u \boldsymbol{\mu}_l^u$ with a fixed coefficient of variance c^u. The relation between independent and dependent flux variables can be obtained via decomposition of the full flux vector into the vectors of independent and dependent flux, and the equation (1) can be expressed as

$$\dot{\boldsymbol{x}}_l = [\boldsymbol{S}^d \quad \boldsymbol{S}^u] \begin{bmatrix} \boldsymbol{v}_l^d \\ \boldsymbol{u}_l \end{bmatrix} = \boldsymbol{S}^d \boldsymbol{v}_l^d + \boldsymbol{S}^u \boldsymbol{u}_l \tag{4}$$

where $m \times \mathrm{rank}(\boldsymbol{S})$ matrix $\boldsymbol{S}^d$ and $m \times f$ matrix $\boldsymbol{S}^u$ contain columns

corresponding to dependent and independent flux variables, respectively. When $\boldsymbol{S}^d$ is regular with $m = \mathrm{rank}(\boldsymbol{S})$ and $\det(\boldsymbol{S}^d) \neq 0$, the full flux vector is directly computed as

$$\begin{aligned}\boldsymbol{v}_l = \begin{bmatrix}\boldsymbol{v}_l^d \\ \boldsymbol{u}_l\end{bmatrix} = \begin{bmatrix}(\boldsymbol{S}^d)^{-1}(\dot{\boldsymbol{x}}_l - \boldsymbol{S}^u\boldsymbol{u}_l) \\ \boldsymbol{u}_l\end{bmatrix} &= \begin{bmatrix}-(\boldsymbol{S}^d)^{-1}\boldsymbol{S}^u \\ \boldsymbol{I}_{r-m}\end{bmatrix}\boldsymbol{u}_l + \begin{bmatrix}(\boldsymbol{S}^d)^{-1} \\ \boldsymbol{0}\end{bmatrix}\dot{\boldsymbol{x}}_l \\ &= \boldsymbol{W}^u\boldsymbol{u}_l + \boldsymbol{W}^{\dot{x}}\dot{\boldsymbol{x}}_l\end{aligned} \tag{5}$$

with transformation matrices $\boldsymbol{W}^u$ and $\boldsymbol{W}^{\dot{x}}$ defined based on the inverse of $\boldsymbol{S}^d$. Here we just considered the metabolic pathways in which the stoichiometric matrix $\boldsymbol{S}^d$ was regular, and in other words the following situation was not considered because the full metabolic fluxes could not be computed from independent flux variables: $r < m$ or linearly dependent rows in $\boldsymbol{S}$ resulting in $\mathrm{rank}(\boldsymbol{S}) < m$. We avoided these conditions by appropriate definition of the target metabolic pathway and stoichiometric matrix.

Now we obtain the prior distribution of the full metabolic fluxes from equation (5). Since linear combination of normal random variables is also normal random variables, the vector of full metabolic flux follows the r-dimensional normal distribution

$$p(\boldsymbol{v}_l|\boldsymbol{u}_l) = \mathcal{N}(\boldsymbol{v}_l|\boldsymbol{\mu}_l^v, \boldsymbol{\Sigma}_l^v) \tag{6}$$

with mean $\boldsymbol{\mu}_l^v = \boldsymbol{W}^u\boldsymbol{\mu}_l^u$ and covariance matrix $\boldsymbol{\Sigma}_l^v = \boldsymbol{W}^u\boldsymbol{\Sigma}_l^u(\boldsymbol{W}^u)^\top + \boldsymbol{W}^{\dot{x}}\boldsymbol{\Sigma}_l^{\dot{x}}(\boldsymbol{W}^{\dot{x}})^\top$. The diagonal covariance matrix $\boldsymbol{\Sigma}_l^{\dot{x}}$ represents the variances around prior metabolite changes. In strict steady state, the prior for metabolite change becomes Dirac's delta function at zero. By increasing the variances, we can relax the steady-state assumption on individual metabolites and encode allowance for accumulations or depletions of them. The squared diagonal element $\boldsymbol{\sigma}_l^{\dot{x}}$ was obtained from the mean of the prior distribution of metabolic flux as

$$\boldsymbol{\sigma}_l^{\dot{x}} = \frac{c^{\dot{x}}}{2}(\boldsymbol{S}^+\boldsymbol{\mu}_l^v + \boldsymbol{S}^-\boldsymbol{\mu}_l^v), \tag{7}$$

by defining production and consumption stoichiometric matrices as,

$$S^+ = \frac{1}{2}(\mathrm{abs}(\boldsymbol{S}) + \boldsymbol{S}), \qquad S^- = \frac{1}{2}(\mathrm{abs}(\boldsymbol{S}) - \boldsymbol{S}), \tag{8}$$

where $\mathrm{abs}(\boldsymbol{S})$ is the matrix of absolute values of the corresponding entries of $\boldsymbol{S}$. Note that the entries of the matrix $\boldsymbol{S}^{+}$ corresponds to the number of molecules of metabolite produced by the reaction. Conversely, each entry of the matrix $\boldsymbol{S}^{-}$ give the number of molecules of metabolite consumed by the reaction.

Next, we define the likelihood of the measured amounts of enzymes given parameters and prior for elasticity coefficients based on linlog kinetics. Since the experimental data of the amounts of metabolites and proteins is usually not available for all reactions in the metabolic network, the likelihood was calculated for a subset of the reactions. The metabolic flux through the subset of the reactions is represented as a $r' \times 1$ vector $\boldsymbol{v}'_l \subset \boldsymbol{v}_l$ ($r' \leq r$). For each sample $k = 1,2,\dots,n_j$ under condition l ($l = 1,2,\dots,g$), the amounts of metabolites $\boldsymbol{x}_{kl}$ (a $m \times 1$ vector) and the amounts of proteins $\boldsymbol{e}_{kl}$ (a $r' \times 1$ vector) are obtained after normalizing by the average amounts across all the conditions. In the linlog kinetics framework, the metabolic flux through reaction j ($j = 1,2,\dots,r'$) $(\hat{v}'_{jkl})$ is expressed as

$$\hat{v}'_{jkl} = v_j^0 e_{jkl}\left(1 + \boldsymbol{\epsilon}_j^{\top} \ln \boldsymbol{x}_{kl}\right), \tag{9}$$

where v_j^0 is the metabolic flux in the reference state, and $\boldsymbol{\epsilon}_j$ is the $m \times 1$ vector of elasticity coefficients. v_j^0 is defined as the mean of the prior metabolic flux values across conditions as $v_j^0 = 1/g \sum_{l=1}^{g} \mu_{jl}^{v'}$ where $\mu_{jl}^{v'}$ is a prior mean of the metabolic flux v'_j. ϵ_{ji} describes the effect of changes of the amounts of metabolites x_i on the metabolic flux v'_j, and is positive if metabolite i is a substrate or an allosteric activator for reaction j, while negative if the metabolite is a product or an allosteric inhibitor. If metabolite i does not directly participate in reaction j, the value of ϵ_{ji} equals to zero. According to equation (9) the amount of the enzyme is calculated using the inferred metabolic flux v'_{jl}. Here, the amount of the enzyme in each sample e_{jkl} is assumed to follow the normal distribution around the estimated value $\hat{e}_{jkl}$, and we obtain the likelihood of the measured amount of the enzyme given parameters as

$$p\left(e_{jkl}\middle|\boldsymbol{x}_{kl}, v'_{jl}, \boldsymbol{\epsilon}_j, \sigma^{\hat{e}}\right) = \mathcal{N}\left(e_{jkl}\middle|\hat{e}_{jkl}, \left(\sigma^{\hat{e}}\right)^2\right),$$
$$\hat{e}_{jkl} = \frac{v'_{jl}}{v_j^0}\frac{1}{1+\boldsymbol{\epsilon}_j^{\top}\ln \boldsymbol{x}_{kl}}, \tag{10}$$

where v'_{jl} is the inferred metabolic flux of reaction j. For simplicity, the variance of the error term $\sigma^{\hat{e}}$ is set to the same values in all the reactions, samples, and conditions. We placed half-Cauchy priors with scale 0.5 on $\sigma^{\hat{e}}$, set as a weakly informative prior distribution given that $\sigma^{\hat{e}}$ was expected to be less than one.

Elasticity coefficients are likely not to significantly deviate from the range between -1 and 1 theoretically (Kacser et al., 1995), and are likely to be positive for substrates and allosteric activators whereas negative for products and allosteric inhibitors. This property generates prior distributions for elasticity coefficients as

$$p(\epsilon_{ji}) = \begin{cases} \mathcal{H}(\epsilon_{ji}|1) & \text{if metabolite } i \text{ is substrate} \\ & \text{or allosteric activator in reaction } j \\ -\mathcal{H}(\epsilon_{ji}|1) & \text{if metabolite } i \text{ is product} \\ & \text{or allosteric inhibitor in reaction } j \\ \delta(\epsilon_{ji}|0) & \text{others} \end{cases} \tag{11}$$

$$\mathcal{H}(x|\sigma) = \frac{\sqrt{2}}{\sigma\sqrt{\pi}}\exp\left(-\frac{x^2}{2\sigma^2}\right), \qquad x \in [0, +\infty)$$

$$\delta(x|\mu) = \lim_{\sigma\to 0}\frac{1}{\sqrt{2\pi\sigma^2}}\exp\left(-\frac{(x-\mu)^2}{2\sigma^2}\right), \qquad x \in (-\infty, +\infty)$$

where $\mathcal{H}(x|\sigma)$ indicates half-normal distribution with variance σ, and $\delta(x|\mu)$ indicates Dirac's delta function equal to zero everywhere except for μ.

The amounts of proteins are explained in the context of not only metabolic flux but also of protein turnover. Here we define the likelihood of the measured amounts of transcripts given parameters and priors for protein turnover coefficient β_{ij}. For each sample $k = 1,2,\ldots,n_j$ under condition l $(l = 1,2,\ldots,g)$, the estimated amounts of proteins $\hat{\boldsymbol{e}}_{kl}$ and the corresponding amounts of transcripts $\hat{\boldsymbol{t}}_{kl}$ represents the protein change rate $\dot{\boldsymbol{e}}_{kl}$ as

$$\dot{\boldsymbol{e}}_{kl} = (\boldsymbol{k}_l^+)^{\top}\hat{\boldsymbol{t}}_{kl} - (\boldsymbol{k}_l^-)^{\top}\hat{\boldsymbol{e}}_{kl}, \tag{12}$$

where $\boldsymbol{k}_l^+$ and $\boldsymbol{k}_l^-$ are $r' \times 1$ vectors of kinetic parameters for protein synthesis and degradation, respectively. Assuming the amounts of proteins as stable within the observed time intervals, the amounts of proteins and transcripts have a linear relationship and we obtain the likelihood of the measured amount of the transcript given parameters as,

$$p\left(t_{jkl} \middle| \hat{e}_{jkl}, \beta_{jl}, \sigma^{\hat{t}}\right) = \mathcal{N}\left(t_{jkl} \middle| \hat{t}_{jkl}, \left(\sigma^{\hat{t}}\right)^2\right),$$
$$\hat{t}_{jkl} = \frac{1}{\beta_{jl}} \hat{e}_{jkl}, \tag{13}$$

using turnover coefficient $\beta_{jl} = k_{jl}^+ / k_{jl}^-$ and the estimated amount of enzyme $\hat{e}_{jkl}$ in each sample defined in equation (10). The parameter to determine the variance of the error term $\sigma^{\hat{t}}$ is simplified as the common values in all the reactions, samples, and conditions. We placed half-Cauchy priors with scale 0.5 on $\sigma^{\hat{t}}$. Given that there is a high correlation between copy numbers of RNA and protein especially in the glucose metabolism (Matsumoto et al., 2017), the turnover coefficient β_{jl} is expected to be close to one when the amounts of proteins and transcripts are normalized to their averages. Therefore, the prior distribution for β_{jl} can be described by

$$p\left(\beta_{jl} \middle| \sigma_l^{\beta}\right) = \mathcal{N}\left(\beta_{jl} \middle| 1, \left(\sigma_l^{\beta}\right)^2\right) \tag{14}$$

with error term defined by σ_l^{β} in each condition. We placed half-Cauchy priors with scale 0.5 on σ_l^{β}.

Combining the likelihood with the priors based on linlog kinetics (Equations 6, 10, 11, and Table S6) and protein turnover (Equations 13, 14, and Table S6), the joint posterior distribution is given by

$$p\left(\boldsymbol{v}, \boldsymbol{\epsilon}, \boldsymbol{\beta} \middle| \boldsymbol{e}, \boldsymbol{x}, \boldsymbol{t}, c^u, c^{\dot{x}}, S\right)$$
$$\propto p\left(\boldsymbol{e}, \boldsymbol{t} \middle| \boldsymbol{x}, \boldsymbol{v}, \boldsymbol{\epsilon}, \sigma^{\hat{e}}, \boldsymbol{\beta}, \sigma^{\hat{t}}\right) p\left(\boldsymbol{v} \middle| \boldsymbol{u}, c^{\dot{x}}, S\right) p\left(\boldsymbol{u} \middle| \boldsymbol{\mu}^u, c^u\right) p(\boldsymbol{\epsilon}) p(\boldsymbol{\beta}) p\left(\sigma^{\hat{e}}\right) p\left(\sigma^{\hat{t}}\right), \tag{15}$$
$$p\left(\boldsymbol{e}, \boldsymbol{t} \middle| \boldsymbol{x}, \boldsymbol{v}, \boldsymbol{\epsilon}, \sigma^{\hat{e}}, \boldsymbol{\beta}, \sigma^{\hat{t}}\right) = p\left(\boldsymbol{e} \middle| \boldsymbol{x}, \boldsymbol{v}, \boldsymbol{\epsilon}, \sigma^{\hat{e}}\right) p\left(\boldsymbol{t} \middle| \boldsymbol{x}, \boldsymbol{v}, \boldsymbol{\epsilon}, \boldsymbol{\beta}, \sigma^{\hat{t}}\right).$$

where $p\left(\boldsymbol{e}, \boldsymbol{t} \middle| \boldsymbol{x}, \boldsymbol{v}, \boldsymbol{\epsilon}, \sigma^{\hat{e}}, \boldsymbol{\beta}, \sigma^{\hat{t}}\right)$ is the likelihood of the measured amounts of enzymes

based on linlog kinetics combined with the likelihood of the measured amounts of transcripts based on protein turnover, $p(\boldsymbol{v}|\boldsymbol{u}, c^{\dot{x}}, S)$ is the prior distribution or metabolic flux $\boldsymbol{v}$, $p(\boldsymbol{u}|\boldsymbol{\mu}^u, c^u)$ is the hyperprior distribution for independent flux $\boldsymbol{u}$, $p(\boldsymbol{\epsilon})$ is the prior distribution for elasticity coefficients $\boldsymbol{\epsilon}$, $p(\boldsymbol{\beta})$ is the prior distribution for protein turnover coefficients $\boldsymbol{\beta}$, $p(\sigma^{\hat{e}})$ is the prior distribution for parameter of error term $\sigma^{\hat{e}}$, and $p(\sigma^{\hat{t}})$ is the prior distribution for parameter of error term $\sigma^{\hat{t}}$.

We applied OMELET to the experimental data from mice in four conditions: WT at fasting state, WT after oral glucose administration, *ob*/*ob* at fasting state, and *ob*/*ob* after oral glucose administration. The independent fluxes were constrained so that the flux through G6PC in WT mice at fasting state was fixed at one. A metabolic flux through each reaction was inferred simultaneously in all the conditions and as inferred as the relative value to that through G6PC in WT mice at fasting state. The amounts of pyruvate and oxaloacetate were not available in our measurements because of their chemical instability and low concentrations. For such metabolite species, the relative amounts normalized to the mean across the conditions were inferred as parameters. The amounts of enzymes of Gpt and Glud1 were not measured and only the likelihood of the measured amounts of transcripts was evaluated. Several enzymes function as complex including succinate dehydrogenase, which is also known as respiratory complex II. Two subunits of succinate dehydrogenase, Sdha and Sdhb, were available both in the amounts of proteins and transcripts. The amounts of Sdha and Sdhb were independently normalized to the mean values across the conditions, and then the product was introduced as $\boldsymbol{e}$ for the reaction through succinate dehydrogenase in equation (10). Other reactions were catalyzed by a single enzyme or by complex with only one subunit measured and a single enzyme data was used.

We performed posterior predictive checks to evaluate the fitting of the model to the measured data of the amounts of enzymes and transcripts from mice. Posterior

predictive distributions of enzymes can be simulated by sampling parameters from the posterior and using them to generate replicate data sets based on equation (10). Posterior predictive distributions of transcripts can be simulated in the same way based on equation (13). We compared the posterior predictive distributions with the measured data and confirmed the good fits to the experimental data of the amounts of enzymes and transcripts (Figure S4).

We also applied OMELET to the simulated data from a kinetic model expressing the yeast glycolysis. The dataset contained the amounts of metabolites, enzymes in five conditions (WT and four mutant strains) described in a later section. Since the amounts of transcripts were not available, we obtained the joint posterior distribution

$$\begin{aligned} &p\left(\boldsymbol{v}, \boldsymbol{\epsilon}, \boldsymbol{\beta} \middle| \boldsymbol{e}, \boldsymbol{x}, c^{u}, c^{\dot{x}}, S\right) \\ &\qquad \propto p\left(\boldsymbol{e} \middle| \boldsymbol{x}, \boldsymbol{v}, \boldsymbol{\epsilon}, \sigma^{\hat{e}}\right) p\left(\boldsymbol{v} \middle| \boldsymbol{u}, c^{\dot{x}}, S\right) p(\boldsymbol{u} | \boldsymbol{\mu}^{u}, c^{u}) p(\boldsymbol{\epsilon}) p(\boldsymbol{\beta}) p\left(\sigma^{\hat{e}}\right) \end{aligned} \tag{16}$$

where the likelihood of transcripts (Table S6) was removed from equation (15). The independent fluxes were constrained so that the metabolic flux through glucose uptake (hexose transporter; HXT) in WT strain was fixed at one. A metabolic flux through each reaction was inferred as the relative value to that through HXT in WT.

Parameter estimation

Based on the specified prior distribution and likelihood, the posterior distributions of parameters were numerically estimated by Markov Chain Monte Carlo (MCMC) sampling. The algorithm was a No-U-turn sampler (NUTS), a variant of Hamiltonian Monte Carlo (HMC), constructing an iterative process that eventually converges to the true posterior distribution (Hoffman and Gelman, 2014). For application to the data from mice, we ran four chains of 20,000 iterations with 10,000 burnings with thinning of 2, resulting in 20,000 samples in total. Convergence of Markov Chains was evaluated by R-hat diagnostic, which compares the between- and within-chain estimated for model

parameters. All our runs satisfied R-hat less than 1.05, indicating that chains were mixed well. All the parameter estimation was performed using RStan library (version 2.19.2) in R software (3.6.1) within a Docker container (Merkel, 2014).

Simulation using kinetic model of yeast glycolysis

The model of yeast glycolysis was downloaded from the public model repository BioModels Database (Le Novère et al., 2006) as SBML (Systems Biology Markup Language) format (Hucka et al., 2003), with the identifier BIOMD0000000503 (Messiha et al., 2014; Smallbone et al., 2013). The kinetic model represented the glycolytic pathway from glucose down to ethanol as well as the pentose phosphate pathway, and only the glycolytic part was used in our simulation. Briefly, we first perturbed the original model (WT) to generate models of four mutant strains (mutant 01 to 04), and then 50 datasets including the amounts of metabolites, enzymes, and metabolic fluxes were generated for each of the models. The parameters of the WT model in enzyme i (z_i^0) to be perturbed included kcat, Vmax, or an enzyme concentration. The magnitude of perturbation ζ_l ($l = 1, \ldots, 5$), strain-specific noise, was set so that mutant strains with perturbed parameter sets $\boldsymbol{z}^l$ were gradually deviated from the WT model (Table S7).

Based on the perturbed model, sample datasets were generated by introducing sample-specific noises $\zeta_i^{\text{sample}} \sim \mathcal{N}\left(0, \left(0.1 z_i^l\right)^2\right)$ for each parameter value z_i^l, which represented variety between samples in the same strain and were assumed to be common in all the strains. Steady-state simulation using the parameter set with the strain-specific and sample-specific noises produced a dataset containing 50 samples with the amounts of metabolites, enzymes, and metabolic fluxes under each of the five conditions. All the steady-state simulation were executed using the Simbiology toolbox in MATLAB (The MathWorks, Inc., Natick, Massachusetts, United States of America).

To evaluate the performance of OMELET, only the dataset of the amounts of enzymes and metabolites, not including metabolic fluxes, were used as input. For MCMC

sampling, we ran four chains of 20,000 iterations with 17,500 burnings with thinning 2, resulting in 5,000 samples in total. The metabolic fluxes inferred by OMELET were then compared with those obtained from the perturbation and steady-state simulation of the kinetic model.

Contributions of regulators to changes in metabolic flux

We define a contribution ψ_{jh} of regulators to changes in metabolic flux between conditions. The regulators include transcripts, unaccounted enzyme regulators, substrates, products, cofactors, allosteric effectors and unaccounted flux regulators. The unaccounted enzyme regulators can include other regulatory mechanisms of the protein amount of enzyme such as protein degradation and stability. The unaccounted flux regulators can include other regulators such as phosphorylation of enzymes and unknown allosteric effectors not included in OMELET. The concept of the contribution is to partition the cause of changes in metabolic flux between conditions into underlying changes in the amounts of regulators including enzymes and metabolites. The contribution was calculated based on propagation of uncertainty of regulators' amounts to metabolic flux, and a similar approach was described in a previous study (Hackett et al., 2016). Note that we analyzed only the local effects of regulators on changes in metabolic flux and do not evaluate the effects on changes in metabolic flux in which the regulator was not directly participated.

Before we calculated the contribution, we define the amounts of unaccounted flux regulators and unaccounted enzyme regulators. Based on equation (9), the inferred metabolic flux through reaction j in condition l can be described as

$$v_{jl} = \hat{v}_{jkl} + \phi^{v}_{jkl} = v^{0}_{j} e_{jkl}\left(1 + \boldsymbol{\epsilon}^{\mathsf{T}}_{j} \ln \boldsymbol{x}_{kl}\right) + \phi^{v}_{jkl}. \quad (17)$$

ϕ^{v}_{jkl} is the amount of an unaccounted flux regulator in sample k in condition l and represents the deviation of the inferred metabolic flux from that calculated using linlog kinetics. Similarly, based on equation (13), the measured amount of enzyme in reaction

j can be described as

$$e_{jkl} = \beta_{jl} t_{jkl} + \phi^{e}_{jkl}. \tag{18}$$

ϕ^{e}_{jkl} is the amount of an unaccounted enzyme regulator and represents the deviation of the measured amount of the enzyme from that calculated using the amount of transcript and the protein turnover coefficient. Combining equations (17) and (18), we obtain

$$v_{jl} = v_j^0 \left(\beta_{jl} t_{jkl} + \phi^{e}_{jkl}\right)\left(1 + \boldsymbol{\epsilon}_j^{\top} \, ln \, \boldsymbol{x}_{kl}\right) + \phi^{v}_{jkl} \tag{19}$$

which represents metabolic flux v_{jl} as a function of the transcript t_{jkl}, the unaccounted enzyme regulator ϕ^{e}_{jkl}, the metabolites $\boldsymbol{x}_{kl}$ including substrates, products, cofactors and allosteric effectors, as well as the unaccounted flux regulator ϕ^{v}_{jkl}.

We defined the contribution to changes in metabolic flux from transcripts, unaccounted enzyme regulators, and metabolites of substrates, products, cofactors and allosteric effectors, as well as unaccounted flux regulators. Based on propagation of uncertainty, assuming that interactions between regulators is ignored, the variance $\mathrm{Var}(v_j)$ of inferred metabolic flux v_j in reaction j can be approximated as

$$\mathrm{Var}(v_j) \approx \sum_h \left(\frac{\partial v_j}{\partial y_{jh}}\right)^2 \mathrm{Var}(y_{jh}) \tag{20}$$

with the amount of regulator h (y_{jh}), the sensitivity of the regulator to the metabolic flux $\partial v_j / \partial y_{jh}$, and the variance of the amount of the regulator $\mathrm{Var}(y_{jh})$. Regulator h is the transcript, the unaccounted enzyme regulator, substrate, product, cofactor, allosteric effector, or unaccounted flux regulator. The variance of the amount of the regulator between two conditions $\mathrm{Var}(y_{jh})$ is expressed as the change in the amount of the regulator between the two conditions Δy_{jh} as

$$\mathrm{Var}(y_{jh}) = \left(\frac{\Delta y_{jh}}{2}\right)^2. \tag{21}$$

The sensitivity for each regulator to the metabolic flux $\partial v_j / \partial y_{jh}$ is defined based on Eq. (17) as

$$\frac{\partial v_j}{\partial y_{jh}} = \begin{cases} \bar{\beta}_j v_j^0 \left(1 + \boldsymbol{\epsilon}_j^{\mathsf{T}} \ln \bar{\boldsymbol{x}}\right) & \text{if regulator } h \text{ is the transcript} \\ v_j^0 \left(1 + \boldsymbol{\epsilon}_j^{\mathsf{T}} \ln \bar{\boldsymbol{x}}\right) & \text{if regulator } h \text{ is the unaccounted enzyme regulator} \\ \dfrac{v_j^0 \bar{\beta}_j \bar{t}_j \epsilon_{ji}}{\overline{y_{jh}}} & \text{if regulator } h \text{ is a metabolite} \\ 1 & \text{if regulator } h \text{ is the unaccounted flux regulator} \end{cases}, \tag{22}$$

where $\bar{\boldsymbol{x}}$, $\bar{e}_j$ and $\bar{t}_j$ indicate the means of the metabolites, enzyme, and transcript in reaction j across two conditions, respectively. Using the variance and the sensitivity of the amount of each regulator, we defined a contribution of the change in regulator h to the change in metabolic flux through reaction j as

$$\psi_{jh} = \frac{\left(\frac{\partial v_j}{\partial y_{jh}}\right)^2 \left(\Delta y_{jh}\right)^2}{\sum_h \left(\frac{\partial v_j}{\partial y_{jh}}\right)^2 \left(\Delta y_{jh}\right)^2}. \tag{23}$$

The contribution was a compositional data whose sum of the contributions of all the regulators to a change in metabolic flux equals one. The contribution ranged from zero to one, and the larger value meant the stronger effect of the regulator to the change in metabolic flux.

The contribution was calculated for changes in metabolic flux through each reaction between each pair of condition (Figure S6); (i) WT and *ob*/*ob* mice at fasting state, (ii) WT and *ob*/*ob* mice after oral glucose administration, (iii) fasting and after oral glucose administration in WT mice and (iv) fasting and after oral glucose administration in *ob*/*ob* mice. Therefore, the calculated contributions represent the extent to which a change in each regulator contributed to the change in metabolic flux between the conditions.

Metabolomic analysis

Metabolomic measurements were performed as previously described (Egami et al., 2021; Kokaji et al., 2020). Total metabolites and proteins were extracted from the liver with

1006 methanol:chloroform:water (2.5:2.5:1) extraction. Approximately 40 mg of the liver was
1007 suspended with 500 μL of ice-cold methanol containing internal standards [20 μM L-
1008 methionine sulfone (Wako), 2-morpholinoethanesulfonic acid (Dojindo), and D-
1009 Camphor-10-sulfonic acid (Wako)] for quantification of metabolites, then with 500 μL of
1010 chloroform, and finally with 200 μL of water. After centrifugation at 4,600 × g for 15 min
1011 at 4°C, the separated aqueous layer was filtered through a 5 kDa cutoff filter (Human
1012 Metabolome Technologies) to remove protein contamination. The filtrate (320 μL) was
1013 lyophilized and, prior to MS analysis, dissolved in 50 μL water containing reference
1014 compounds [200 μM each of trimesic acid (Wako) and 3-aminopyrrolidine (Sigma-
1015 Aldrich)]. Proteins were precipitated by addition of 800 μL of ice-cold methanol to the
1016 interphase and organic layers and centrifuged at 12,000 × g for 15 min at 4°C. The pellet
1017 was washed with 1 mL of ice-cold 80% (v/v) methanol and resuspended in 1 mL of sample
1018 buffer containing 1% SDS and 50 mM Tris-Cl pH8.8, followed by sonication. The total
1019 protein concentration was determined by bicinchoninic acid (BCA) assay and was used
1020 for normalization of metabolite concentration among samples.

1021 All CE-MS experiments were performed using an Agilent 1600 Capillary
1022 Electrophoresis system (Agilent technologies), an Agilent 6230 TOF LC/MS system, an
1023 Agilent 1200 series isocratic pump, a G1603A Agilent CE-MS adapter kit, and a G1607A
1024 Agilent CE electrospray ionization (ESI)-MS sprayer kit. Briefly, to analyze cationic
1025 compounds, a fused silica capillary [50 μm internal diameter (i.d.) × 100 cm] was used
1026 with 1 M formic acid as the electrolyte (Soga and Heiger, 2000). Methanol/water (50%
1027 v/v) containing 0.01 μM hexakis(2,2-difluoroethoxy)phosphazene was delivered as the
1028 sheath liquid at 10 μL/min. ESI-TOFMS was performed in positive ion mode, and the
1029 capillary voltage was set to 4 kV. Automatic recalibration of each acquired spectrum was
1030 achieved using the masses of the reference standards ([^{13}C isotopic ion of a protonated
1031 methanol dimer $(2CH_3OH+H)]^+$, *m/z* 66.0631) and ([hexakis(2,2-
1032 difluoroethoxy)phosphazene $+H]^+$, *m/z* 622.0290). The metabolites were identified by

1033 comparing their m/z values and relative migration times to the metabolite standards.
1034 Quantification was performed by comparing peak areas to calibration curves generated
1035 using internal standardization techniques with methionine sulfone. The other conditions
1036 were identical to those described previously (Soga et al., 2006). To analyze anionic
1037 metabolites, a commercially available COSMO(+) (chemically coated with cationic
1038 polymer) capillary (50 μm i.d. × 105 cm) (Nacalai Tesque, Kyoto, Japan) was used with
1039 a 50 mM ammonium acetate solution (pH 8.5) as the electrolyte. Methanol/5 mM
1040 ammonium acetate (50% v/v) containing 0.01 μM hexakis(2,2-
1041 difluoroethoxy)phosphazene was delivered as the sheath liquid at 10 μL/min. ESI-
1042 TOFMS was performed in negative ion mode, and the capillary voltage was set to 3.5 kV.
1043 Automatic recalibration of each acquired spectrum was achieved using the masses of the
1044 reference standards ([^{13}C isotopic ion of a deprotonated acetate dimer ($2CH_3COOH$-H)]$^-$,
1045 *m*/*z* 120.0384) and ([hexakis(2,2-difluoroethoxy)phosphazene +deprotonated acetate
1046 (CH_3COOH-H)]$^-$, *m*/*z* 680.0355). For anion analysis, D-camphor-10-sulfonic acid were
1047 used as the internal standards. The other conditions were identical to those described
1048 previously (Soga et al., 2009). The acquired raw data were analyzed using our proprietary
1049 software (Sugimoto et al., 2010).
1050
1051
1052 **Proteomic analysis**
1053 *Sample preparation of proteomic analysis*
1054 Sample preparation of proteome analysis were performed as described, previously
1055 (Matsumoto et al., 2017). Frozen powder of liver and muscle were lysed with a solution
1056 containing 2% SDS, 7 M urea, and 100 mM Tris-HCl, pH 8.8, and then subjected to
1057 ultrasonic treatment (five times for 30 s with intervals of 30 s) with a Bioruptor
1058 (Diagenode). The samples were diluted with an equal volume of water. The protein
1059 concentrations of the samples were determined with BCA assays (Bio-Rad), after which

1060 portions (200 μg of protein) were subjected to methanol–chloroform precipitation. The
1061 resulting pellet was dissolved in digestion buffer (0.5 M triethylammonium bicarbo
1062 nate containing 7 M guanidine hydroxide) and heated at 56 °C for 30 min. Each sample
1063 was diluted with an equal volume of water, after which portions were subjected to BCA
1064 assays. The remaining solution (50 μl) was diluted with 50 μl of water and subjected to
1065 digestion with lysyl-endopeptidase (2 μg, Wako) for 4 h at 37 °C. After the addition of
1066 100 μl of water, the samples were further digested with trypsin (2 μg, Thermo Fisher) for
1067 14 h at 37 °C. To block cysteine/cystine residues, we treated the digest with 0.625 mM
1068 Tris(2-carboxyethyl)phosphine hydrochloride (Thermo Fisher) for 30 min at 37 °C, then
1069 performed alkylation with 3.125 mM 2-iodoacetoamide (Sigma) for 30 min at room tem
1070 perature and quenching with 2.5 mM N-acetyl-l-cysteine (Sigma). The resulting digests
1071 were freeze-dried and then labeled with the mTRAQΔ0 reagent (SCIEX). For a deep
1072 proteomics, tryptic digests were separated into 6 fractions with off-Line high-pH reverse
1073 phase chromatography (Matsumoto et al., 2017).
1074
1075 *DDA of peptides for multiple reaction monitoring (MRM) method development*
1076 Target proteins were selected from the proteins listed in three Kyoto Encyclopedia of
1077 Genes and Genomes (KEGG) pathways; Glycolysis / Gluconeogenesis (mmu00010),
1078 Citrate cycle (mmu 00020), and Starch and sucrose metabolism (mmu 00500), and
1079 proteins related to insulin signaling. A key step for the establishment of a successful
1080 targeted proteomic analysis is the accurate selection of proteotypic peptides (PTPs) for
1081 the targets of interest. Therefore, we first performed a discovery phase aimed at the
1082 selection of PTPs, which was based on a deep proteomic characterization of total protein
1083 extract of the murine liver and muscle. mTRAQ-labeled peptides as mentioned above
1084 were fractionated by reversed-phase chromatography on a 16-cm column (inner diameter,
1085 100 μm) packed in house with 2-μm L-column C18 material (CERI). Peptides were eluted
1086 with a linear gradient (typically 5–45% B for 40 min, 45–95% B for 1 min, and 95% B

1087 for 10 min, where A was 0.1% formic acid and 2% acetonitrile, and B was 0.1% formic
1088 acid and 90% acetonitrile), at a flow rate of 200 nl/min. The high-performance LC system
1089 (Eksigent nano-LC) was coupled to a TripleTOF5600 hybrid mass spectrometer (SCIEX).
1090 Data acquisition was performed in IDA mode with the iTRAQ option. Survey MS spectra
1091 were acquired for 100 ms, and the 10 most intense ions were isolated and then fragmented
1092 with an automatically optimized collision energy for an MS/MS acquisition time of 100
1093 ms. Peak lists (mgf) generated by the AB SCIEX MS Data Converter were used to search
1094 a database containing IPI mouse version 3.44 (55 078 protein entries; IPI, European
1095 Bioinformatics Institute) protein sequences concatenated with decoy sequences, with the
1096 use of the MASCOT algorithm (Matrix Science). The search was conducted with the
1097 following parameter settings: trypsin was selected as the enzyme used, the allowed
1098 number of missed cleavages was set to two, and the mTRAQΔ0 label on the NH2-
1099 terminal or lysine residues and carbamidomethylation of cysteine were selected as fixed
1100 modifications. Oxidized methionine and the mTRAQΔ0 label on tyrosine were searched
1101 as variable modifications. The precursor mass tolerance was 50 p.p.m., and the tolerance
1102 of MS/MS ions was 0.02 mass/charge (m/z) units. We imported all significant peptide-
1103 spectrum matches (PSMs) (MASCOT score >20) into a relational database written in
1104 MySQL. From this dataset, we preferentially selected PTP candidates which met the
1105 following criteria: 1. more than six amino acids; 2. absence of tryptic missed-cleavage
1106 sites; 3. The C-terminus of PTPs is Lys or Arg; 4. absence of methionine residues. To
1107 verify whether these PTP candidates were actually identified and quantified in our MRM
1108 systems, trypsin digests used in "DDA of peptides for MRM method development" were
1109 labeled with either mTRAQΔ0 or mTRAQΔ4 and subjected to MRM assays. All MRM
1110 traces were analyzed by iMPAQT-quant (Matsumoto et al., 2017). Peak groups were
1111 scored on the basis of cosine similarity with MS/MS spectra obtained in DDA, peak
1112 coelution of at least three fragment ions for each peptide, the presence or absence of
1113 interfering ions, and intensity. Finally, we selected 2-3 PTPs per target protein and

1114 purchased from Funakoshi Co. All PTPs were resuspended with 20%-50% ethanol,
1115 pooled and labeled with mTRAQΔ4 using standard procedures.
1116
1117 *MRM analysis*
1118 MRM analysis was performed with a QTRAP5500 instrument (SCIEX) equipped with
1119 nano-Advance UHPLC (MICHROM) and HTS-PAL/xt autosampler (CTC Analytics AG).
1120 Peptides were eluted with a linear gradient of 5%–30% B for 45 min, 30%–95% B for 46
1121 min (where A is 0.1% formic acid and B is acetonitrile) at a flow rate of 200 nL/min.
1122 Parameters were set as follows: spray voltage, 2,000 V; curtain gas setting, 10; collision
1123 gas setting, high; ion-source gas-1 setting, 30 and interface-heater temperature, 150 °C.
1124 Collision energy (CE) was calculated with the following formulae: CE = (0.044 × m/z1)
1125 + 5.5 and CE = (0.051 × m/z1) + 0.5 (where m/z1 is the m/z of the precursor ion) for
1126 doubly and triply charged precursor ions, respectively. Collision-cell exit potential (CXP)
1127 was calculated according to the formula: CXP = (0.0391 × m/z2) − 2.2334 (where m/z2
1128 is the m/z of the fragment ion). The declustering potential (DP) was set to 50, and the
1129 entrance potential (EP) was set to 10. Resolution for Q1 and Q3 was set to 'unit' (half-
1130 maximal peak width of 0.7 m/z). The scheduled MRM option was used for all data
1131 acquisition, with a target scan time of 2.0 s and MRM detection windows of 300s. More
1132 than three technical repeats were performed per sample. Raw data were analyzed by
1133 iMPAQT-Quant (Matsumoto et al., 2017) with the corresponding spectra library. Peak
1134 groups were scored on the basis of cosine similarity with the MS/MS spectra obtained in
1135 DDA, a peak co-elution of at least three fragment ions for each peptide, the presence or
1136 absence of interfering ions, and the intensity. Finally, all traces were manually checked to
1137 eliminate inadequate transitions. All quantified transitions were normalized across
1138 samples and converted into protein abundance by SRMstats software on R (Surinova et
1139 al., 2013).
1140

1141 **Transcriptomic analysis**

1142 Transcriptomic measurements were performed as previously described (Egami et al.,
1143 2021; Kokaji et al., 2020). Briefly, total RNA was extracted from the liver using RNeasy
1144 Mini Kit (QIAGEN) and QIAshredder (QIAGEN) and assessed for quantity using
1145 Nanodrop (Thermo Fisher Scientific) and for quality using the 2100 Bioanalyzer (Agilent
1146 Technologies). cDNA libraries were prepared using SureSelect strand-specific RNA
1147 library preparation kit (Agilent Technologies). The resulting cDNAs were subjected to
1148 100-bp paired-end sequencing on an Illumina HiSeq2500 Platform (Illumina)
1149 (Matsumoto et al., 2007). Sequences were aligned to the mouse reference genome
1150 obtained from Ensembl database (Cunningham et al., 2015; Flicek et al., 2014)
1151 (GRCm38/mm10, Ensembl release 70) using the software package TopHat (Trapnell et
1152 al., 2009, 2012) (v.2.0.9), software in the Tuxedo tool. Cufflinks (v.2.2.1), software in the
1153 Tuxedo tool, was used to assemble transcript models from aligned sequences and to
1154 estimate the number of transcripts as an indicator of gene expression. The number of
1155 transcripts was shown as fragments per kilobase of exon per million mapped fragments.

1156

1157 **Blood glucose**

1158 The blood and insulin data at 0, 2, 5, 10, 15, 20, 30, 45, 60, 90, 120, 180, 240 minutes
1159 after oral glucose administration were previously reported (Kokaji et al., 2020).

1160

1161 **QUANTIFICATION AND STATISTICAL ANALYSIS**

1162 For the metabolites, proteins, and transcripts, we defined increased and decreased
1163 molecules between the conditions using the following procedure (Figure 2; Table S2). For
1164 each molecule, we calculated the fold change of the mean amount of WT mice at fasting
1165 state, *ob*/*ob* mice at fasting state, and *ob*/*ob* mice after oral glucose administration over
1166 the mean amount of WT mice at fasting state. The significance of changes was tested by
1167 two-tailed Welch's t-test for each molecule. The q values were calculated by Benjamini-

1168 Hochberg procedure. Molecules that showed an q value less than 0.05 are defined as
1169 significantly changed molecules. Among them, molecules with a fold change larger than
1170 1.5 were defined as increased molecules between the conditions, whereas molecules with
1171 a fold change smaller than 0.67 were defined as decreased molecules. The Pearson
1172 correlation coefficient was calculated between the medians of metabolic fluxes inferred
1173 by OMELET and the means of metabolic fluxes simulated by the kinetic model (Figure
1174 S3C) or in the previous studies (Figures S5B and S5D) across all the reactions in all the
1175 conditions. The p-value was computed by transforming the correlation to create a t
1176 statistic having N-2 degree of freedom, where N is the number of samples.

1177 **REFERNCES**

1178 Burgess, S.C., Jeffrey, F.M.H., Storey, C., Milde, A., Hausler, N., Merritt, M.E.,
1179 Mulder, H., Holm, C., Sherry, A.D., and Malloy, C.R. (2005). Effect of murine strain on
1180 metabolic pathways of glucose production after brief or prolonged fasting. Am. J.
1181 Physiol. Metab. *289*, E53–E61.

1182 Burgess, S.C., Merritt, M.E., Jones, J.G., Browning, J.D., Sherry, A.D., and Malloy,
1183 C.R. (2015). Limitations of detection of anaplerosis and pyruvate cycling from
1184 metabolism of [1-13 C] acetate. Nat. Med. *21*, 108–109.

1185 Cunningham, F., Amode, M.R., Barrell, D., Beal, K., Billis, K., Brent, S., Carvalho-
1186 Silva, D., Clapham, P., Coates, G., Fitzgerald, S., et al. (2015). Ensembl 2015. Nucleic
1187 Acids Res. *43*, D662–D669.

1188 Egami, R., Kokaji, T., Hatano, A., Yugi, K., Eto, M., Morita, K., Ohno, S., Fujii, M.,
1189 Hironaka, K., Uematsu, S., et al. (2021). Trans-omic analysis reveals obesity-associated
1190 dysregulation of inter-organ metabolic cycles between the liver and skeletal muscle.
1191 iScience *24*, 102217.

1192 Erion, D.M., Ignatova, I.D., Yonemitsu, S., Nagai, Y., Chatterjee, P., Weismann, D.,
1193 Hsiao, J.J., Zhang, D., Iwasaki, T., Stark, R., et al. (2009). Prevention of Hepatic
1194 Steatosis and Hepatic Insulin Resistance by Knockdown of cAMP Response Element-
1195 Binding Protein. Cell Metab. *10*, 499–506.

1196 Everett, L.J., Lay, J.L., Lukovac, S., Bernstein, D., Steger, D.J., Lazar, M.A., and
1197 Kaestner, K.H. (2013). Integrative genomic analysis of CREB defines a critical role for
1198 transcription factor networks in mediating the fed/fasted switch in liver. BMC
1199 Genomics *14*, 337.

1200 Flicek, P., Amode, M.R., Barrell, D., Beal, K., Billis, K., Brent, S., Carvalho-Silva, D.,
1201 Clapham, P., Coates, G., Fitzgerald, S., et al. (2014). Ensembl 2014. Nucleic Acids Res.
1202 *42*, D749–D755.

1203 Hackett, S.R., Zanotelli, V.R.T., Xu, W., Goya, J., Park, J.O., Perlman, D.H., Gibney,

P.A., Botstein, D., Storey, J.D., and Rabinowitz, J.D. (2016). Systems-level analysis of mechanisms regulating yeast metabolic flux. Science (80-.). *354*, aaf2786.

Han, H.S., Kang, G., Kim, J.S., Choi, B.H., and Koo, S.H. (2016). Regulation of glucose metabolism from a liver-centric perspective. Exp. Mol. Med. *48*, 1–10.

Hanson, R.W., and Reshef, L. (1997). Regulation of Phosphoenolpyruvate carbozykinase (GTP) gene expression. Annu. Rev. Biochem. *66*, 581–611.

Hasenour, C.M., Wall, M.L., Ridley, D.E., Hughey, C.C., James, F.D., Wasserman, D.H., and Young, J.D. (2015). Mass spectrometry-based microassay of 2H and 13C plasma glucose labelling to quantify liver metabolic fluxes in vivo. Am. J. Physiol. - Endocrinol. Metab. *309*, E191–E203.

Hasenour, C.M., Rahim, M., and Young, J.D. (2020). In Vivo Estimates of Liver Metabolic Flux Assessed by 13C-Propionate and 13C-Lactate Are Impacted by Tracer Recycling and Equilibrium Assumptions. Cell Rep. *32*, 107986.

Heinonen, M., Osmala, M., Mannerström, H., Wallenius, J., Kaski, S., Rousu, J., and Lähdesmäki, H. (2019). Bayesian metabolic flux analysis reveals intracellular flux couplings. Bioinformatics *35*, i548–i557.

Herzig, S., Long, F., Jhala, U.S., Hedrick, S., Quinn, R., Bauer, A., Rudolph, D., Schutz, G., Yoon, C., Puigserver, P., et al. (2001). CREB regulates hepatic gluconeogenesis through the coactivator PGC-1. Nature *413*, 179–183.

Hoffman, M.D., and Gelman, A. (2014). The no-U-turn sampler: Adaptively setting path lengths in Hamiltonian Monte Carlo. J. Mach. Learn. Res. *15*, 1593–1623.

Hucka, M., Finney, A., Sauro, H.M., Bolouri, H., Doyle, J.C., Kitano, H., Arkin, A.P., Bornstein, B.J., Bray, D., Cornish-Bowden, A., et al. (2003). The systems biology markup language (SBML): A medium for representation and exchange of biochemical network models. Bioinformatics *19*, 524–531.

Jang, C., Chen, L., and Rabinowitz, J.D. (2018). Metabolomics and Isotope Tracing. Cell *173*, 822–837.

1231 Jin, E.S., Uyeda, K., Kawaguchi, T., Burgess, S.C., Malloy, C.R., and Sherry, D.D.
1232 (2003). Increased hepatic fructose 2,6-bisphosphate after an oral glucose load does not
1233 affect gluconeogenesis. J. Biol. Chem. *278*, 28427–28433.
1234 Jin, E.S., Beddow, S.A., Malloy, C.R., and Samuel, V.T. (2013). Hepatic glucose
1235 production pathways after three days of a high-fat diet. Metabolism. *62*, 152–162.
1236 John, P.C.S., Strutz, J., Broadbelt, L.J., Tyo, K.E.J., and Bomble, Y.J. (2019). Bayesian
1237 inference of metabolic kinetics from genome-scale multiomics data. PLoS Comput.
1238 Biol. *15*, 1–23.
1239 Kacser, H., Burns, J.A., Felltt, D.A., and Fell, D.A. (1995). The Control of Flux: 21
1240 Years On The control of flux. Pharmaceuticals 18–1995.
1241 Kahn, S.E., Hull, R.L., and Utzschneider, K.M. (2006). Mechanisms linking obesity to
1242 insulin resistance and type 2 diabetes. Nature *444*, 840–846.
1243 Kawata, K., Hatano, A., Yugi, K., Kubota, H., Sano, T., Fujii, M., Tomizawa, Y.,
1244 Kokaji, T., Tanaka, K.Y., Uda, S., et al. (2018). Trans-omic Analysis Reveals Selective
1245 Responses to Induced and Basal Insulin across Signaling, Transcriptional, and
1246 Metabolic Networks. iScience *7*, 212–229.
1247 Kokaji, T., Hatano, A., Ito, Y., Yugi, K., Eto, M., Morita, K., Ohno, S., Fujii, M.,
1248 Hironaka, K.I., Egami, R., et al. (2020). Transomics analysis reveals allosteric and gene
1249 regulation axes for altered hepatic glucose-responsive metabolism in obesity. Sci.
1250 Signal. *13*, eaaz1236.
1251 Matsumoto, M., Pocai, A., Rossetti, L., DePinho, R.A., and Accili, D. (2007). Impaired
1252 Regulation of Hepatic Glucose Production in Mice Lacking the Forkhead Transcription
1253 Factor Foxo1 in Liver. Cell Metab. *6*, 208–216.
1254 Matsumoto, M., Matsuzaki, F., Oshikawa, K., Goshima, N., Mori, M., Kawamura, Y.,
1255 Ogawa, K., Fukuda, E., Nakatsumi, H., Natsume, T., et al. (2017). A large-scale
1256 targeted proteomics assay resource based on an in vitro human proteome. Nat. Methods
1257 *14*, 251–258.

Merkel, D. (2014). Docker: Lightweight Linux Containers for Consistent Development and Deployment. Linux J. *2014*.

Messiha, H.L., Kent, E., Malys, N., Carroll, K.M., Swainston, N., Mendes, P., and Smallbone, K. (2014). Enzyme characterisation and kinetic modelling of the pentose 1 phosphate pathway in yeast 2 network-scale models by merging smaller pathway-scale models. PeerJ Prepr. *2*, e146v4.

Le Novère, N., Bornstein, B., Broicher, A., Courtot, M., Donizelli, M., Dharuri, H., Li, L., Sauro, H., Schilstra, M., Shapiro, B., et al. (2006). BioModels Database: a free, centralized database of curated, published, quantitative kinetic models of biochemical and cellular systems. Nucleic Acids Res. *34*, D689–D691.

Ohno, S., Quek, L.E., Krycer, J.R., Yugi, K., Hirayama, A., Ikeda, S., Shoji, F., Suzuki, K., Soga, T., James, D.E., et al. (2020). Kinetic Trans-omic Analysis Reveals Key Regulatory Mechanisms for Insulin-Regulated Glucose Metabolism in Adipocytes. IScience *23*, 101479.

Patterson, R.E., Kalavalapalli, S., Williams, C.M., Nautiyal, M., Mathew, J.T., Martinez, J., Reinhard, M.K., McDougall, D.J., Rocca, J.R., Yost, R.A., et al. (2016). Lipotoxicity in steatohepatitis occurs despite an increase in tricarboxylic acid cycle activity. Am. J. Physiol. - Endocrinol. Metab. *310*, E484–E494.

Perry, R.J., Borders, C.B., Cline, G.W., Zhang, X.M., Alves, T.C., Petersen, K.F., Rothman, D.L., Kibbey, R.G., and Shulman, G.I. (2016). Propionate increases hepatic pyruvate cycling and anaplerosis and alters mitochondrial metabolism. J. Biol. Chem. *291*, 12161–12170.

Petersen, K.F., Blair, J.B., and Shulman, G.I. (1995). Triiodothyronine treatment increases substrate cycling between pyruvate carboxylase and malic enzyme in perfused rat liver. Metab. - Clin. Exp. *44*, 1380–1383.

Previs, S.F., and Kelley, D.E. (2015). Tracer-based assessments of hepatic anaplerotic and TCA cycle flux: Practicality, stoichiometry, and hidden assumptions. Am. J.

1285 Physiol. - Endocrinol. Metab. *309*, E727–E735.
1286 Roden, M., and Shulman, G.I. (2019). The integrative biology of type 2 diabetes. Nature
1287 *576*, 51–60.
1288 Saa, P.A., and Nielsen, L.K. (2016). Construction of feasible and accurate kinetic
1289 models of metabolism: A Bayesian approach. Sci. Rep. *6*, 29635.
1290 Samuel, V.T., Beddow, S.A., Iwasaki, T., Zhang, X.M., Chu, X., Still, C.D., Gerhard,
1291 G.S., and Shulman, G.I. (2009). Fasting hyperglycemia is not associated with increased
1292 expression of PEPCK or G6Pc in patients with type 2 diabetes. Proc. Natl. Acad. Sci. U.
1293 S. A. *106*, 12121–12126.
1294 Satapati, S., Sunny, N.E., Kucejova, B., Fu, X., He, T.T., Méndez-Lucas, A., Shelton,
1295 J.M., Perales, J.C., Browning, J.D., and Burgess, S.C. (2012). Elevated TCA cycle
1296 function in the pathology of diet-induced hepatic insulin resistance and fatty liver. J.
1297 Lipid Res. *53*, 1080–1092.
1298 Smallbone, K., Messiha, H.L., Carroll, K.M., Winder, C.L., Malys, N., Dunn, W.B.,
1299 Murabito, E., Swainston, N., Dada, J.O., Khan, F., et al. (2013). A model of yeast
1300 glycolysis based on a consistent kinetic characterisation of all its enzymes. FEBS Lett.
1301 *587*, 2832–2841.
1302 Soga, T., and Heiger, D.N. (2000). Amino Acid Analysis by Capillary Electrophoresis
1303 Electrospray Ionization Mass Spectrometry. Anal. Chem. *72*, 1236–1241.
1304 Soga, T., Baran, R., Suematsu, M., Ueno, Y., Ikeda, S., Sakurakawa, T., Kakazu, Y.,
1305 Ishikawa, T., Robert, M., Nishioka, T., et al. (2006). Differential metabolomics reveals
1306 ophthalmic acid as an oxidative stress biomarker indicating hepatic glutathione
1307 consumption. J. Biol. Chem. *281*, 16768–16776.
1308 Soga, T., Igarashi, K., Ito, C., Mizobuchi, K., Zimmermann, H.P., and Tomita, M.
1309 (2009). Metabolomic profiling of anionic metabolites by capillary electrophoresis mass
1310 spectrometry. Anal. Chem. *81*, 6165–6174.
1311 Soltis, A.R., Kennedy, N.J., Xin, X., Zhou, F., Ficarro, S.B., Yap, Y.S., Matthews, B.J.,

1312 Lauffenburger, D.A., White, F.M., Marto, J.A., et al. (2017). Hepatic Dysfunction
1313 Caused by Consumption of a High-Fat Diet. Cell Rep. *21*, 3317–3328.
1314 Sugimoto, M., Wong, D.T., Hirayama, A., Soga, T., and Tomita, M. (2010). Capillary
1315 electrophoresis mass spectrometry-based saliva metabolomics identified oral, breast and
1316 pancreatic cancer-specific profiles. Metabolomics *6*, 78–95.
1317 Sunny, N.E., Parks, E.J., Browning, J.D., and Burgess, S.C. (2011). Excessive hepatic
1318 mitochondrial TCA cycle and gluconeogenesis in humans with nonalcoholic fatty liver
1319 disease. Cell Metab. *14*, 804–810.
1320 Surinova, S., Hüttenhain, R., Chang, C.-Y., Espona, L., Vitek, O., and Aebersold, R.
1321 (2013). Automated selected reaction monitoring data analysis workflow for large-scale
1322 targeted proteomic studies. Nat. Protoc. *8*, 1602–1619.
1323 Trapnell, C., Pachter, L., and Salzberg, S.L. (2009). TopHat: discovering splice
1324 junctions with RNA-Seq. Bioinformatics *25*, 1105–1111.
1325 Trapnell, C., Roberts, A., Goff, L., Pertea, G., Kim, D., Kelley, D.R., Pimentel, H.,
1326 Salzberg, S.L., Rinn, J.L., and Pachter, L. (2012). Differential gene and transcript
1327 expression analysis of RNA-seq experiments with TopHat and Cufflinks. Nat. Protoc. *7*,
1328 562–578.
1329 Turner, S.M., Linfoot, P.A., Neese, R.A., and Hellerstein, M.K. (2005). Sources of
1330 plasma glucose and liver glycogen in fasted ob/ob mice. Acta Diabetol. *42*, 187–193.
1331 Wang, Y., Kwon, H., Su, X., and Wondisford, F.E. (2020). Glycerol not lactate is the
1332 major net carbon source for gluconeogenesis in mice during both short and prolonged
1333 fasting. Mol. Metab. *31*, 36–44.
1334 Yugi, K., Kubota, H., Toyoshima, Y., Noguchi, R., Kawata, K., Komori, Y., Uda, S.,
1335 Kunida, K., Tomizawa, Y., Funato, Y., et al. (2014). Reconstruction of insulin signal
1336 flow from phosphoproteome and metabolome data. Cell Rep. *8*, 1171–1183.
1337 Yugi, K., Kubota, H., Hatano, A., and Kuroda, S. (2016). Trans-Omics: How To
1338 Reconstruct Biochemical Networks Across Multiple “Omic” Layers. Trends

1339 Biotechnol. *34*, 276–290.

1340

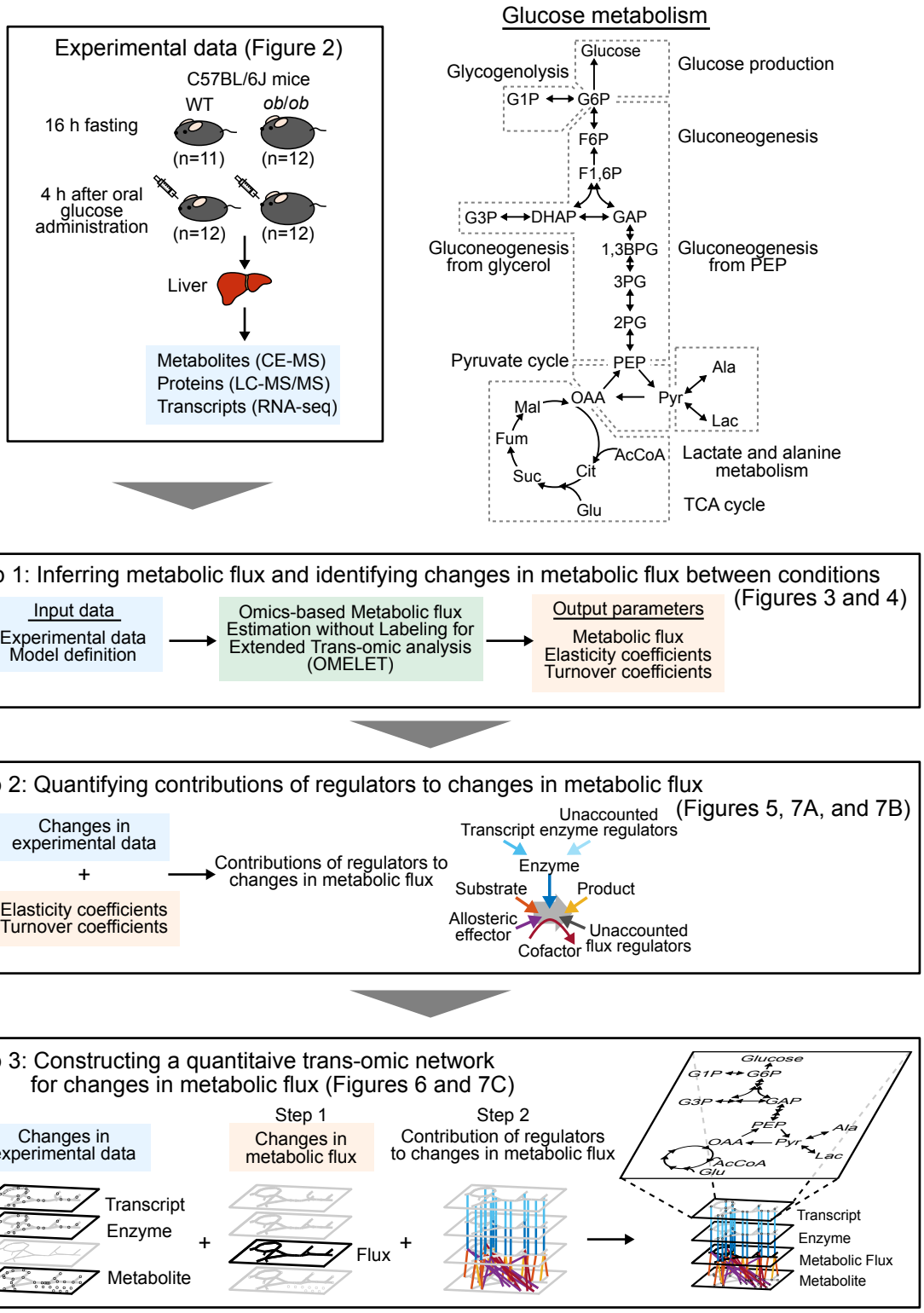
Experimental data (Figure 2)
C57BL/6J mice
WT
ob/ob
16 h fasting
(n=11)
(n=12)
4 h after oral glucose administration
(n=12)
(n=12)
Liver
Metabolites (CE-MS)
Proteins (LC-MS/MS)
Transcripts (RNA-seq)
Glucose metabolism
Glucose
Glycogenolysis
Glucose production
G1P
G6P
F6P
Gluconeogenesis
F1,6P
G3P
DHAP
GAP
Gluconeogenesis from glycerol
1,3BPG
Gluconeogenesis from PEP
3PG
2PG
Pyruvate cycle
PEP
Ala
OAA
Pyr
Mal
Lac
Fum
AcCoA
Lactate and alanine metabolism
Suc
Cit
Glu
TCA cycle
Step 1: Inferring metabolic flux and identifying changes in metabolic flux between conditions (Figures 3 and 4)
Input data
Experimental data
Model definition
Omics-based Metabolic flux Estimation without Labeling for Extended Trans-omic analysis (OMELET)
Output parameters
Metabolic flux
Elasticity coefficients
Turnover coefficients
Step 2: Quantifying contributions of regulators to changes in metabolic flux (Figures 5, 7A, and 7B)
Changes in experimental data
+
Elasticity coefficients
Turnover coefficients
Contributions of regulators to changes in metabolic flux
Unaccounted Transcript enzyme regulators
Enzyme
Substrate
Product
Allosteric effector
Cofactor
Unaccounted flux regulators
Step 3: Constructing a quantitaive trans-omic network for changes in metabolic flux (Figures 6 and 7C)
Changes in experimental data
Step 1
Changes in metabolic flux
Step 2
Contribution of regulators to changes in metabolic flux
Transcript
Enzyme
Metabolite
+
Flux
+
Transcript
Enzyme
Metabolic Flux
Metabolite

Figure 1. Overview of OMELET.

The procedures consist of three steps by inferring metabolic fluxes in the glucose metabolism in each condition, identifying changes in metabolic flux between the conditions, and quantifying contributions of the regulators to changes in metabolic flux between the conditions. Abbreviations of the metabolites on the map of glucose metabolism are described in Table S1.

Figure 2

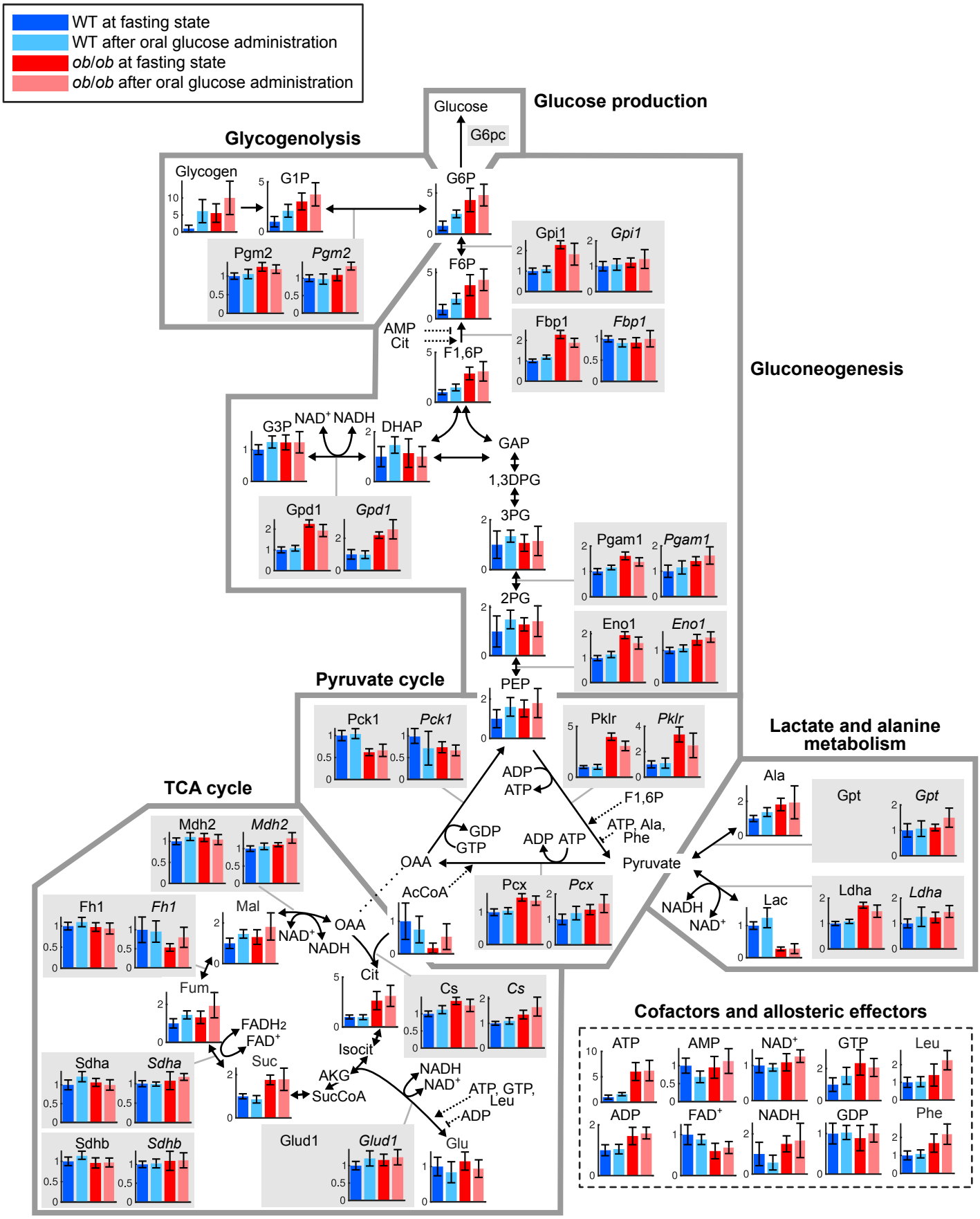
WT at fasting state
WT after oral glucose administration
ob/ob at fasting state
ob/ob after oral glucose administration
Glucose production
Glucose
G6pc
Glycogenolysis
Glycogen
G1P
G6P
Pgm2
Pgm2
Gpi1
Gpi1
F6P
Fbp1
Fbp1
AMP
Cit
F1,6P
Gluconeogenesis
G3P
NAD+ NADH
DHAP
GAP
1,3DPG
Gpd1
Gpd1
3PG
Pgam1
Pgam1
2PG
Eno1
Eno1
PEP
Pyruvate cycle
Pck1
Pck1
Pklr
Pklr
ADP
ATP
F1,6P
ATP, Ala, Phe
GDP
GTP
ADP ATP
OAA
Pyruvate
AcCoA
Pcx
Pcx
Lactate and alanine metabolism
Ala
Gpt
Gpt
NADH
NAD+
Lac
Ldha
Ldha
TCA cycle
Mdh2
Mdh2
Fh1
Fh1
Mal
NAD+
NADH
OAA
Cit
Cs
Cs
Fum
FADH2
FAD+
Isocit
Sdha
Sdha
Suc
AKG
SucCoA
NADH
NAD+
ATP, GTP, Leu
ADP
Sdhb
Sdhb
Glud1
Glud1
Glu
Cofactors and allosteric effectors
ATP
AMP
NAD+
GTP
Leu
ADP
FAD+
NADH
GDP
Phe

Figure 2. Metabolomic, proteomic and transcriptomic data in the glucose metabolism in liver of WT and *ob*/*ob* mice at fasting state and after oral glucose administration.

Measured molecules (metabolites, proteins and transcripts) mapped on the glucose metabolism in liver. On the map the irreversible reactions are described as one-headed arrows, whereas the reversible reactions are described as double-headed arrows. Allosteric activation and inhibition are described as dotted one-headed and dotted bar-headed arrows, respectively. Each box contains four bar plots corresponding to four different conditions: WT at fasting state (blue), WT after oral glucose administration (light blue), *ob*/*ob* at fasting state (red) and *ob*/*ob* after oral glucose administration (pink). The bars and error bars in each molecule represent the mean ± SD normalized to the mean of the data from WT at fasting state. Abbreviations of metabolites, proteins and transcripts are described in Table S2. See also Figure S1.

Figure 3

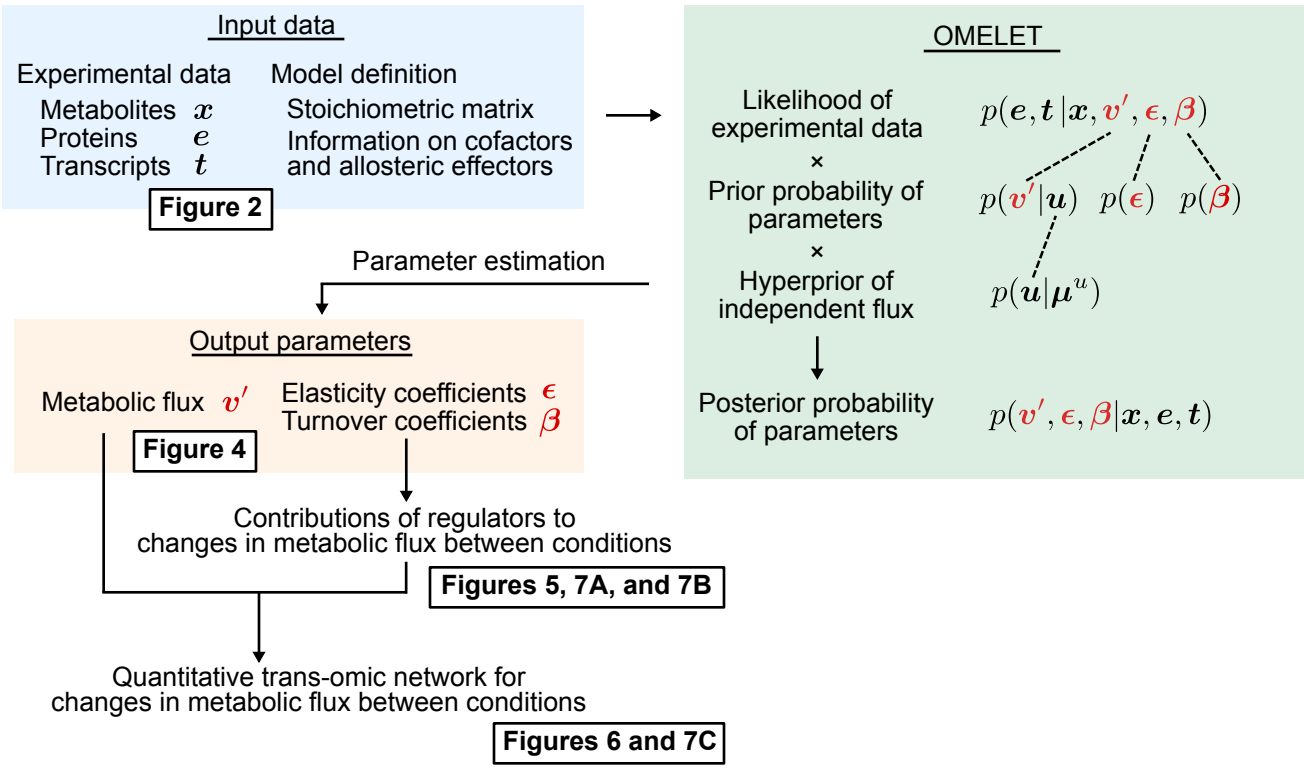
Input data
Experimental data
Metabolites $\boldsymbol{x}$
Proteins $\boldsymbol{e}$
Transcripts $\boldsymbol{t}$
Model definition
Stoichiometric matrix
Information on cofactors and allosteric effectors
Figure 2
OMELET
Likelihood of experimental data
$p(\boldsymbol{e}, \boldsymbol{t} | \boldsymbol{x}, \boldsymbol{v}', \boldsymbol{\epsilon}, \boldsymbol{\beta})$
×
Prior probability of parameters
$p(\boldsymbol{v}'|\boldsymbol{u})$ $p(\boldsymbol{\epsilon})$ $p(\boldsymbol{\beta})$
×
Hyperprior of independent flux
$p(\boldsymbol{u}|\boldsymbol{\mu}^u)$
Posterior probability of parameters
$p(\boldsymbol{v}', \boldsymbol{\epsilon}, \boldsymbol{\beta}|\boldsymbol{x}, \boldsymbol{e}, \boldsymbol{t})$
Parameter estimation
Output parameters
Metabolic flux $\boldsymbol{v}'$
Elasticity coefficients $\boldsymbol{\epsilon}$
Turnover coefficients $\boldsymbol{\beta}$
Figure 4
Contributions of regulators to changes in metabolic flux between conditions
Figures 5, 7A, and 7B
Quantitative trans-omic network for changes in metabolic flux between conditions
Figures 6 and 7C

Figure 3. Workflow for the inference of metabolic flux by OMELET

Overview of the workflow for the inference of metabolic flux. Shaded rectangles represent the inputs (light blue), OMELET (light green) and the outputs (orange). The output parameters are colored in red. See also Figures S2, S3 and Materials and Methods.

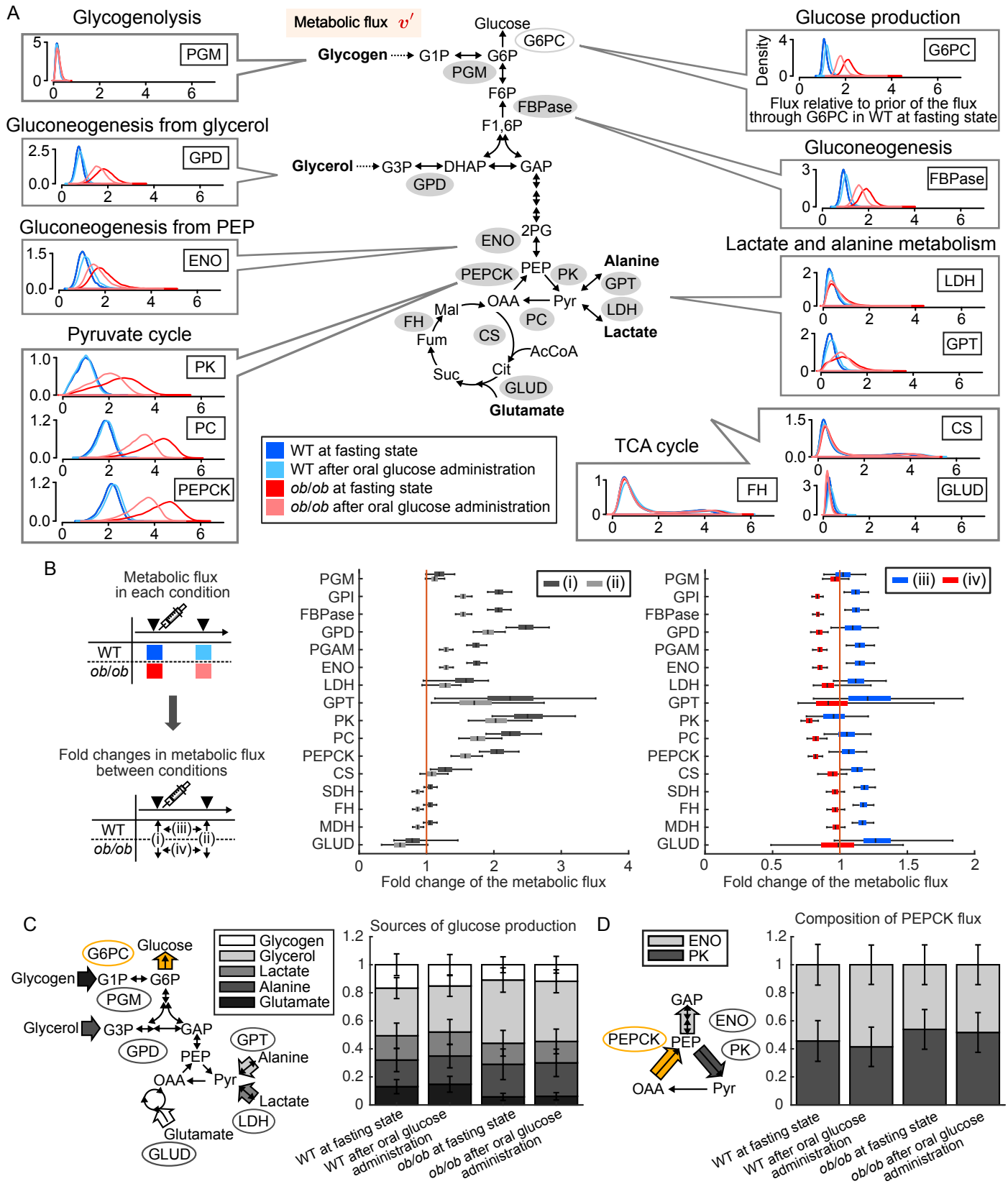
A
Glycogenolysis
PGM
Gluconeogenesis from glycerol
GPD
Gluconeogenesis from PEP
ENO
Pyruvate cycle
PK
PC
PEPCK
Metabolic flux v'
Glucose
G6PC
Glycogen
G1P
G6P
PGM
F6P
FBPase
F1,6P
Glycerol
G3P
DHAP
GAP
GPD
2PG
ENO
PEP
PEPCK
PK
Alanine
GPT
OAA
Pyr
LDH
Lactate
Mal
FH
Fum
CS
PC
AcCoA
Cit
Suc
GLUD
Glutamate
WT at fasting state
WT after oral glucose administration
ob/ob at fasting state
ob/ob after oral glucose administration
Glucose production
G6PC
Density
Flux relative to prior of the flux through G6PC in WT at fasting state
Gluconeogenesis
FBPase
Lactate and alanine metabolism
LDH
GPT
TCA cycle
FH
CS
GLUD
B
Metabolic flux in each condition
WT
ob/ob
Fold changes in metabolic flux between conditions
(i)
(ii)
(iii)
(iv)
PGM
GPI
FBPase
GPD
PGAM
ENO
LDH
GPT
PK
PC
PEPCK
CS
SDH
FH
MDH
GLUD
Fold change of the metabolic flux
C
Glucose
G6PC
Glycogen
G1P
G6P
PGM
Glycerol
G3P
GAP
GPD
PEP
OAA
Pyr
GPT
Alanine
Lactate
LDH
Glutamate
GLUD
Glycogen
Glycerol
Lactate
Alanine
Glutamate
Sources of glucose production
WT at fasting state
WT after oral glucose administration
ob/ob at fasting state
ob/ob after oral glucose administration
D
ENO
PK
GAP
PEPCK
PEP
OAA
Pyr
Composition of PEPCK flux

Figure 4. Inference of metabolic fluxes in the glucose metabolism in liver of WT and *ob*/*ob* mice at fasting state and after oral glucose administration.

(A) Posterior distributions of the metabolic fluxes in the glucose metabolism. Each box contains four density plots corresponding to four different conditions: WT at fasting state (blue), WT after oral glucose administration (light blue), *ob*/*ob* at fasting state (red) and *ob*/*ob* after oral glucose administration (pink). A metabolic flux through each reaction is inferred relative to the mean of the prior for the metabolic flux through G6PC in WT mice at fasting state. Only the representative reactions (shaded gray circles in the map) in each pathway were presented. See also Table S4.

(B) Fold changes of the metabolic flux of *ob*/*ob* mice over that of WT mice at fasting state (i) and after oral glucose administration (ii) in each reaction, and fold changes of the metabolic flux after oral glucose administration over that at fasting state in WT mice (iii) and *ob*/*ob* mice (iv) in each reaction. The median of the posterior predictive distribution in the OMELET model is represented by a black line within the box for each reaction, the box extends from the lower to the 25th and 75th percentiles, and the whiskers extend to 2.5^{th} and 97.5^{th} percentiles to cover 95% of the data. The samples outside the range of adjacent values are not displayed. The vertical orange line indicates the boundary where a fold change equals one.

(C) Sources of glucose production. The stacked bars and error bars represent the mean ± SD of the proportions of glycogen, glycerol, lactate, alanine and glutamate to the glucose production. The proportions of the sources are calculated from the proportion of metabolic fluxes through PGM, GPD, LDH, GPT and GLUD, respectively (black circle) to that through G6PC (yellow circle).

(D) Composition of the metabolic flux through PEPCK. The stacked bars and error bars represent the mean ± SD of the proportions of the metabolic fluxes through ENO and PK to that through PEPCK.

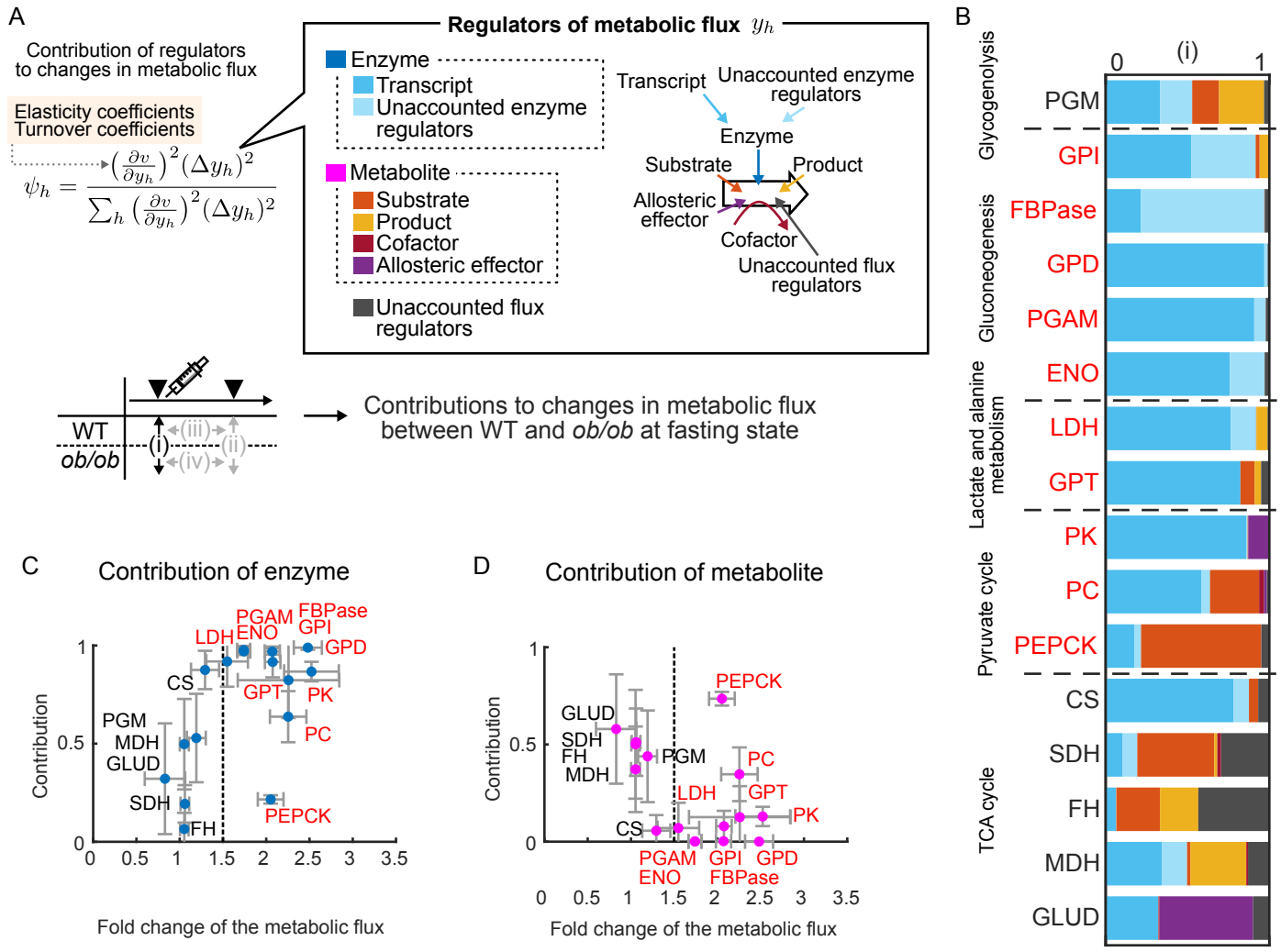
A
Contribution of regulators to changes in metabolic flux
Elasticity coefficients
Turnover coefficients
$\psi_h = \frac{\left(\frac{\partial v}{\partial y_h}\right)^2 (\Delta y_h)^2}{\sum_h \left(\frac{\partial v}{\partial y_h}\right)^2 (\Delta y_h)^2}$
Regulators of metabolic flux y_h
Enzyme
Transcript
Unaccounted enzyme regulators
Metabolite
Substrate
Product
Cofactor
Allosteric effector
Unaccounted flux regulators
Transcript
Unaccounted enzyme regulators
Enzyme
Substrate
Product
Allosteric effector
Cofactor
Unaccounted flux regulators
WT
ob/ob
(i)
(ii)
(iii)
(iv)
Contributions to changes in metabolic flux between WT and ob/ob at fasting state
B
(i)
0
1
Glycogenolysis
Gluconeogenesis
Lactate and alanine metabolism
Pyruvate cycle
TCA cycle
PGM
GPI
FBPase
GPD
PGAM
ENO
LDH
GPT
PK
PC
PEPCK
CS
SDH
FH
MDH
GLUD
C
Contribution of enzyme
Contribution
Fold change of the metabolic flux
D
Contribution of metabolite
Contribution
Fold change of the metabolic flux

Figure 5. Contributions of regulators to changes in metabolic flux between fasting WT and *ob*/*ob* mice.

(A) Schematic representation of contributions of regulators to changes in metabolic flux between conditions. The contribution was defined based on the sensitivity of regulators to metabolic flux, which is calculated using the elasticity coefficients and turnover coefficients, and changes in the amounts of regulators between the conditions following the method previously described (Hackett et al., 2016). The regulators of metabolic flux were enzyme (blue) including transcript (light blue) and unaccounted enzyme regulator (azure), metabolite (pink) including substrate (orange), product (yellow), cofactor (red) and allosteric effectors (purple), and unaccounted flux regulators (gray). See also Materials and Methods.

(B) Contribution of regulators to changes in metabolic flux between WT and *ob*/*ob* mice at fasting state (i). The reactions with the fold changes of the metabolic flux of *ob*/*ob* mice over that of WT mice at fasting state larger than 1.5 are highlighted in red. The stacked bars indicate the mean of the contributions independently calculated in all the Markov chain Monte Carlo samples in Figure S6 (i). See also Table S5.

(C, D) Scatter plots illustrating the relationships between the contributions of enzyme (C) or metabolite (D) to changes in metabolic flux and the fold changes of the metabolic flux of *ob*/*ob* mice over that of WT mice at fasting state. For each reaction, the mean ± SD of the distribution of the contributions of enzyme or metabolite to changes in metabolic flux (x-axis) is plotted against the mean ± SD of the distribution of the fold changes of the metabolic flux of *ob*/*ob* mice over that of WT mice at fasting state (y-axis). The vertical gray dotted line indicates the boundary where a fold change equals 1.5. The reactions with the fold changes of the metabolic flux of *ob*/*ob* mice over that of WT mice at fasting state larger than 1.5 are highlighted in red. See also Tables S4 and S5.

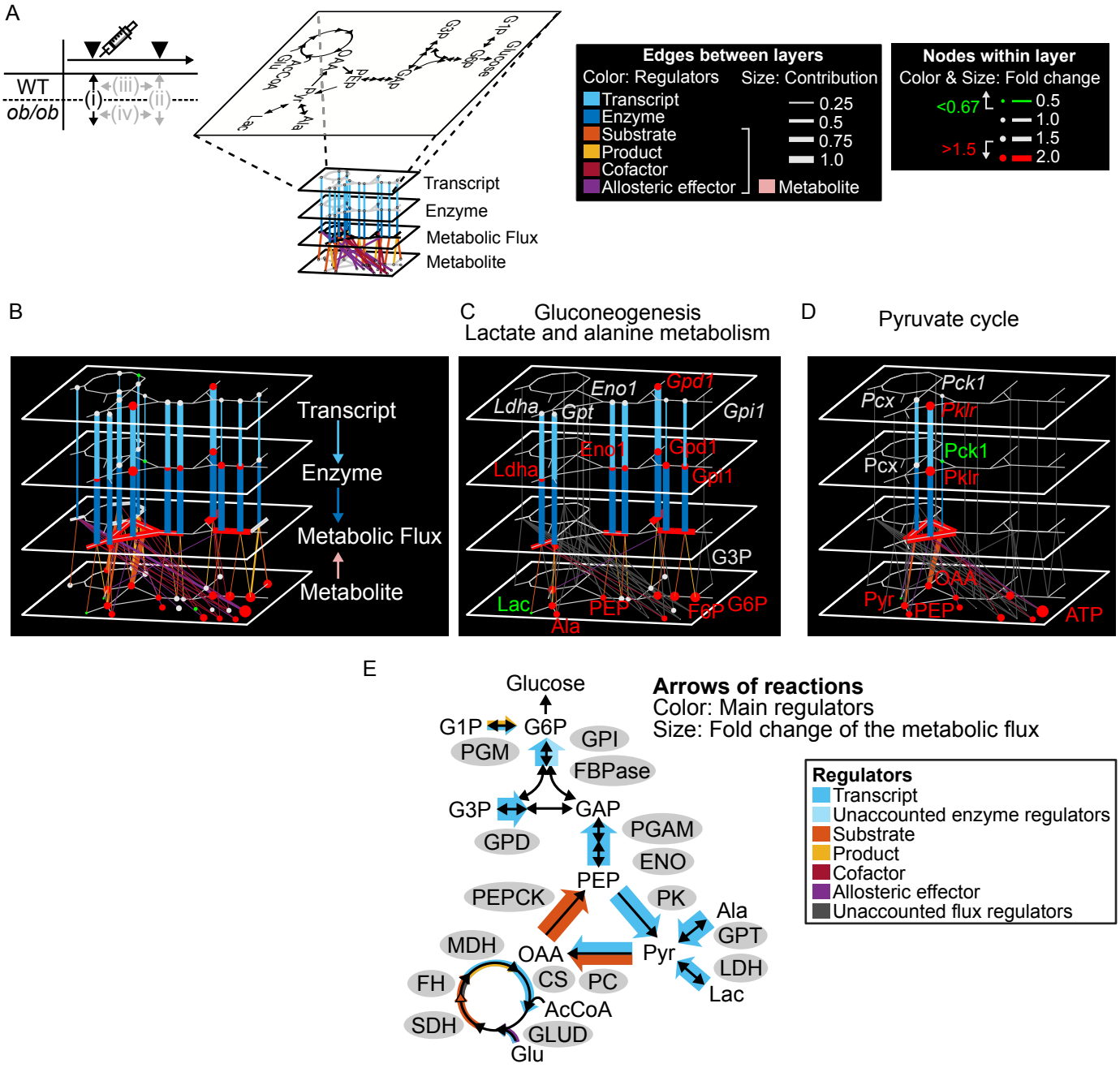
A
WT
ob/ob
(i)
(ii)
(iii)
(iv)
Transcript
Enzyme
Metabolic Flux
Metabolite
Edges between layers
Color: Regulators
Size: Contribution
Transcript
Enzyme
Substrate
Product
Cofactor
Allosteric effector
0.25
0.5
0.75
1.0
Metabolite
Nodes within layer
Color & Size: Fold change
<0.67
>1.5
0.5
1.0
1.5
2.0
B
Transcript
Enzyme
Metabolic Flux
Metabolite
C
Gluconeogenesis
Lactate and alanine metabolism
Ldha
Gpt
Eno1
Gpd1
Gpi1
G3P
Lac
Ala
PEP
Fdp
G6P
D
Pyruvate cycle
Pck1
Pcx
Pklr
OAA
Pyr
PEP
ATP
E
Glucose
G1P
G6P
PGM
GPI
FBPase
G3P
GAP
GPD
PGAM
ENO
PEP
PEPCK
PK
Ala
GPT
MDH
OAA
Pyr
LDH
FH
CS
PC
Lac
AcCoA
SDH
GLUD
Glu
Arrows of reactions
Color: Main regulators
Size: Fold change of the metabolic flux
Regulators
Transcript
Unaccounted enzyme regulators
Substrate
Product
Cofactor
Allosteric effector
Unaccounted flux regulators

Figure 6. Quantitative trans-omic networks for changes in metabolic flux between WT and *ob*/*ob* mice at fasting state.

The quantitative trans-omic network consisted of four layers (Transcript, Enzyme, Metabolic Flux and Metabolite). Nodes in Transcript, Enzyme and Metabolite layer (circles) represented the transcripts, proteins and metabolites. Nodes in Metabolic Flux layer (lines within layer) represented the reactions. Edges from Transcript layer to Enzyme layer represented regulation of enzyme by transcript, and those by unaccounted enzyme regulators were not displayed. Edges from Enzyme layer to Metabolic Flux layer represented contributions of enzyme to changes in metabolic flux between the conditions. Edges from Metabolite layer to Metabolic Flux layer represent regulation of changes in metabolic flux by metabolites as substrate, product, cofactor, and allosteric effector. Unaccounted flux regulators were not displayed. The size of nodes represents fold changes of corresponding molecules of *ob*/*ob* mice over those of WT mice. The colors of the nodes are determined by fold changes as red (fold change > 1.5), light green (fold change < 0.67), and gray. See also Tables S2 and S4. The sizes of the edges represent contributions of regulators to changes in metabolic flux. The colors of the edges represent regulators including transcript (light blue), enzyme (blue), substrate (orange), product (yellow), cofactor (red), allosteric effector (purple). See also Table S5. The subnetworks are extracted from the full network (B): the subnetwork of gluconeogenesis and lactate and alanine metabolism (C), and that of pyruvate cycle (D). The simplified metabolic pathway with metabolic fluxes and the contributions of main regulators is displayed (E). The color of the arrow in each reaction indicates the main regulators which we defined as those with contribution is larger than 0.25. The size of the arrow in each reaction indicates fold changes of the metabolic flux of *ob*/*ob* mice over those of WT mice.

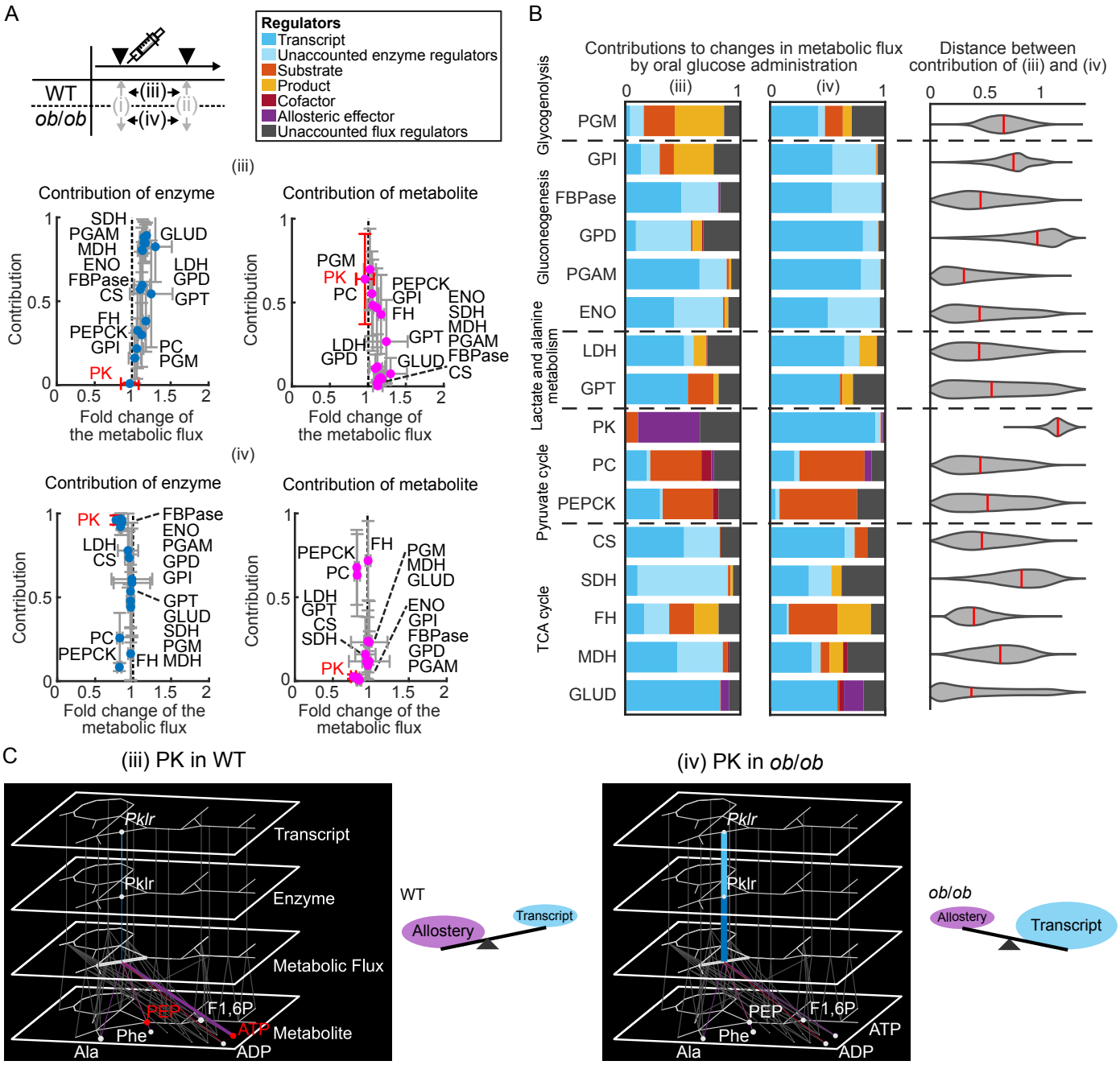
A
WT
ob/ob
(iii)
(iv)
Regulators
Transcript
Unaccounted enzyme regulators
Substrate
Product
Cofactor
Allosteric effector
Unaccounted flux regulators
Contribution of enzyme
Contribution of metabolite
Contribution
Fold change of the metabolic flux
B
Contributions to changes in metabolic flux by oral glucose administration
Distance between contribution of (iii) and (iv)
Glycogenolysis
Gluconeogenesis
Lactate and alanine metabolism
Pyruvate cycle
TCA cycle
PGM
GPI
FBPase
GPD
PGAM
ENO
LDH
GPT
PK
PC
PEPCK
CS
SDH
FH
MDH
GLUD
C
(iii) PK in WT
(iv) PK in ob/ob
Pklr
Transcript
Enzyme
Metabolic Flux
Metabolite
PEP
F1,6P
ATP
Phe
Ala
ADP
WT
Allostery
Transcript
ob/ob

Figure 7. Contributions of regulators to changes in metabolic flux through PK by oral glucose administration.

(A) Scatter plots illustrating the relationships between the contributions of enzyme (blue) and metabolite (pink) to changes in metabolic flux and the fold changes of the metabolic flux after oral glucose administration over that at fasting state in WT mice (iii) and *ob*/*ob* mice (iv). For each reaction, the mean ± SD of the distribution of the contributions of enzyme or metabolite to changes in metabolic flux (x-axis) is plotted against the mean ± SD of the distribution of the fold changes of the metabolic flux of *ob*/*ob* mice over that of WT mice at fasting state (y-axis). The vertical gray dotted line indicates the boundary where a fold change equals one. PK is highlighted in red.

(B) Contribution of regulators to changes in metabolic flux between fasting and after oral glucose administration in WT mice (iii) and *ob*/*ob* mice (iv). The stacked bars indicate the mean of the contributions independently calculated in all the Markov chain Monte Carlo samples in Figures S6 (iii) and (iv). The violin plot in each reaction represents the distribution of the distance quantified as L2 norm between the contribution in WT mice (iii) and *ob*/*ob* mice (iv) independently calculated in all the Markov chain Monte Carlo samples. The vertical red line in each violin plot means the median of the distribution. See also Table S5.

(C) Quantitative trans-omic networks for changes in metabolic flux through PK by oral glucose administration in WT mice (iii) and *ob*/*ob* mice (iv). The networks had the same structures as those in Figure 6. Schematic representation of the main regulators to changes in metabolic flux between fasting and after oral glucose administration was displayed on the right side of the quantitative trans-omic network. We considered F1,6P as an allosteric activator, and ATP, alanine and phenylalanine as allosteric inhibitors for PK in Metabolite layer.